ARTICLES

Photonic band structures of one- and two-dimensional periodic systems with metallic components in the presence of dissipation

V. Kuzmiak* and A. A. Maradudin
Department of Physics and Astronomy, University of California, Irvine, California 92697
(Received 30 October 1996)

We present an approach that allows calculating photonic band structures of electromagnetic waves propagating in periodic systems containing dispersive and highly absorptive materials characterized by a dielectric function, which is frequency dependent and has a non-negligible imaginary part. This method, which provides a complementary approach to that of the transfer-matrix method, is based on the use of a position-dependent dielectric function and the plane-wave technique. The use of the complex form of the dielectric function transforms Maxwell's equations into a generalized nonlinear eigenvalue problem. At low filling fractions of the dispersive and absorptive component ($f \leqslant 1\%$), the generalized eigenvalue problem is reduced to a problem of solving sets of simultaneous nonlinear equations which correspond to the diagonal terms of the matrix equation in the plane-wave representation, with the nondiagonal elements taken into account perturbatively. The resulting complex band structure yields, in addition to the dispersion curves, the attenuation of each mode as it propagates through the system. We first consider a model system represented by a one-dimensional (1D) periodic array of alternating layers of vacuum, and a metal characterized by the complex frequency-dependent dielectric function. To calculate the photonic band structure of this system we employ, in addition to the transfer-matrix method and our perturbative plane-wave approach, a standard linearization technique which solves the general nonlinear eigenvalue problem by the diagonalization of an equivalent, enlarged, matrix. We then apply both our perturbative plane-wave approach and the linearization scheme to obtain the photonic band structures of an infinite array of parallel, infinitely long metallic rods whose intersections with a perpendicular plane form a simple square lattice. The interesting features associated with the presence of dissipation displayed by the photonic band structures, such as an asymmetric behavior of the absorption coefficient and the lifetime of each electromagnetic wave for wave vectors near the Brillouin-zone boundaries, the splitting of the lifetimes of degenerate modes, and the different dependences of the real and imaginary parts of the complex photonic band structure on the polarization of the electromagnetic waves in 2D systems, are discussed. [S0163-1829(97)07711-4]

I. INTRODUCTION

In recent years the propagation of electromagnetic (EM) waves in periodic dielectric structures has received much experimental and theoretical attention. The photonic band structures of these systems exhibit intervals of frequencies in which EM waves are forbiddeen—photonic band gaps—which can open up under favorable circumstances. The existence of the photonic band gaps can lead to a variety of interesting phenomena of both fundamental and practical interest, and has potential applications in many scientific and technical areas.[1]

To date, theoretical calculations of the dispersion relation for propagation of EM waves in two-dimensional (2D) and 3D periodic media have been carried out for purely dielectric, periodic media, whose components are characterized by dielectric functions, that are real, positive, and frequency-independent.[2–23] Interest in the nature of the photonic band structures of periodic systems containing components fabricated from metallic and semiconducting materials has led recently to several theoretical investigations.[24–33] Both the plane-wave technique and the transfer-matrix approach[10] have been applied successfully to the calculation of the photonic band structures of EM waves propagating in 2D and 3D periodic systems, with components characterized by real, frequency-dependent, dielectric functions, and in systems constructed from dispersive and highly absorptive materials characterized by a dielectric function that is frequency-dependent and has a non-negligible imaginary part. Such an investigation is directly related to the experimental effort to create ordered dielectric materials with band gaps in the visible region of the optical spectrum, since in this region some materials have frequency-dependent dielectric constants and/or are highly absorbing. In the near-infrared and visible regions various types of lasers and detectors can be used to observe a rich variety of both linear and nonlinear phenomena.[34,35]

The use of the plane-wave technique for the calculation of the photonic band structures of systems that contain components characterized by frequency-dependent, complex dielectric functions presents a more challenging problem than does its use in the case of purely dielectric materials, since it requires the solution of a generalized nonlinear eigenvalue problem. This eigenvalue problem can be solved by a linear-

ization scheme, which requires the diagonalization of an equivalent, enlarged matrix.[36,37] To incorporate the specific nature of the frequency-dependent dielectric function an alternative, plane-wave approach was published recently by the present authors,[27] in which the generalized eigenvalue problem is reduced to the problem of diagonalizing of a set of matrices whose size equals the number of plane waves kept in the expansions for the components of the electromagnetic field in the system.

The aim of this paper is to present an approach, developed within the framework of the plane-wave technique, which allows calculating photonic band structures of periodic systems containing components that are characterized by a complex, frequency-dependent, dielectric function. Our approach provides an alternative method to that based on the highly computer-intensive linearization scheme. Both methods are employed to explore how the photonic band structures in 1D and 2D periodic systems with metallic components are affected by the presence of dissipation. In the case of 1D lattices the transfer-matrix method is also used to calculate the dispersion curves and the absorption coefficents of the modes.

If dissipation is introduced into the metallic components of a periodic array of slabs (rods) through the use of a complex dielectric function of the form

$$\epsilon(\omega)=1-\frac{\omega_p^2}{\omega(\omega+i\gamma)}, \tag{1.1}$$

where ω_p is the plasma frequency of the conduction electrons and $\gamma=1/\tau_e$ is an inverse electron relaxation time, the problem of obtaining the photonic band structure cannot be reduced to the solution of a single standard eigenvalue problem, but it can be transformed into a generalized nonlinear eigenvalue problem. The use of the standard linearization scheme leads to the diagonalization of high-dimensional equivalent matrix whose eigenvalues are complex. For low filling fractions of the dispersive and absorptive component ($f\leqslant 0.01$), the generalized nonlinear eigenvalue problem can be reduced to a solution of a set of uncoupled nonlinear equations, which correspond to the diagonal terms of the matrix equation in the plane-wave representation, with the nondiagonal elements taken into account perturbatively. The resulting complex band structure yields, in addition to the dispersion curves, the attenuation of each mode as it propagates through the system.

We start in Sec. II by considering a model system represented by a one-dimensional, periodic array of alternating layers of vacuum and metallic slabs characterized by the complex dielectric function given by Eq. (1.1). Both our perturbative plane-wave approach and the linearization technique are used to calculate the complex photonic band structures. In addition to these techniques, the transfer-matrix method is also employed to calculate the dispersion curves and the absorption coefficients of the modes. In Sec. III we apply our method to obtain the photonic band structures of an infinite array of parallel, infinitely long metallic rods, whose intersections with a perpendicular plane form a square lattice. To assess the reliability and accuracy of our method we also carry out a numerical computation of the photonic band structure of the infinite system consisting of metallic rods arrayed in the square lattice by using the linearization scheme. The results obtained by the use of transfer-matrix method within the context of 1D systems and the approaches based on the plane-wave approximation in both 1D and 2D systems considered in this paper are presented in Sec. IV. In Sec. V we discuss the results obtained, present possible directions for future research, and summarize the conclusions of this work.

II. ONE-DIMENSIONAL SYSTEM-METALLIC SLABS IN THE PRESENCE OF DISSIPATION

A. Reduction to a set of simultaneous nonlinear equations

We begin by formulating the problem of obtaining the photonic band structures of one-dimensional periodic structures. The physical system we consider consists of alternating layers of vacuum and a metal characterized by the frequency-dependent dielectric function $\epsilon(\omega)$ given by Eq. (1.1). We consider s polarized (TE) waves assumed to propagate along the x_1 axis, whose electric vector is parallel to the x_2 axis. The intersections of the axes of the slabs with the x_1 axis form a one-dimensional lattice whose sites are given by the points $x(l)=la$, where a is the lattice constant, while l is an arbitrary positive or negative integer, or zero. The ratio of the thickness of the metallic layers to the period of the lattice is the filling fraction $f=2R/a$, where $d=2R$ is the thickness of the metal layer, and takes values in the range $(0, a)$. Because the dielectric function $\epsilon(x|\omega)$ of this system is a position-dependent, periodic function of x_1, with the period given by the lattice constant a,

$$\epsilon(x_1+a|\omega)=\epsilon(x_1|\omega), \tag{2.1}$$

it may be expanded in a one-dimensional Fourier series according to

$$\epsilon(x_1|\omega)=\sum_G \hat{\epsilon}(G)e^{iGx_1}, \tag{2.2}$$

where $G=2\pi n/a$, $n=0,\pm 1,\pm 2,\ldots,$ and

$$\hat{\epsilon}(G)=1-f\frac{\omega_p^2}{\omega(\omega+i\gamma)} \quad G=0 \tag{2.3a}$$

$$=-f\frac{\omega_p^2}{\omega(\omega+i\gamma)}\frac{\sin(GR)}{(GR)} \quad G\neq 0. \tag{2.3b}$$

In the case of s polarization, we seek solutions of the Maxwell equations which have the forms

$$\mathbf{E}(\mathbf{x};t)=(0,E(x_1|\omega),0)\exp(-i\omega t), \tag{2.4a}$$

$$\mathbf{H}(\mathbf{x};t)=(0,0,H(x_1|\omega))\exp(-i\omega t). \tag{2.4b}$$

The Maxwell curl equations for the two nonzero field components are

$$\frac{d}{dx_1}E(x_1|\omega)=i\frac{\omega}{c}H(x_1|\omega), \tag{2.5a}$$

$$\frac{d}{dx_1}H(x_1|\omega)=i\frac{\omega}{c}D(x_1|\omega)=i\frac{\omega}{c}\epsilon(x_1|\omega)E(x_1|\omega). \tag{2.5b}$$

When we eliminate $H(x_1|\omega)$ from these equations, we obtain the equation satisfied by $E(x_1|\omega)$, which we write in the form

$$\frac{d^2}{dx_1^2}E(x_1|\omega)+\epsilon(x_1|\omega)\frac{\omega^2}{c^2}E(x_1|\omega)=0. \tag{2.6}$$

Since $\epsilon(x_1|\omega)$ is unchanged by translation through a lattice constant a, we can also expand $E(x_1|\omega)$ in a form

$$E(x_1|\omega)=\sum_G B(k|G)e^{i(k+G)x_1}. \tag{2.7}$$

To solve Eq. (2.6) we substitute the expansions (2.2) and (2.7) into Eq. (2.6), and obtain the equation satisfied by the coefficients $\{B(k|G)\}$,

$$(k+G)^2B(k|G)=\frac{\omega^2}{c^2}\hat{\epsilon}(0)B(k|G)+\frac{\omega^2}{c^2}{\sum_{G'}}'\,\hat{\epsilon}(G-G')B(k|G'), \tag{2.8}$$

where the prime on the sum over G' indicates that the term with $G'=G$ is omitted. At this point we define a complex variable

$$\mu=\frac{\omega}{c}. \tag{2.9}$$

Then use of the results for $\hat{\epsilon}(G)$ given by Eqs. (2.3) transforms Eq. (2.8) into the following equation:

$$\left(\mu^3+i\frac{\gamma}{c}\mu^2-\mu\left[(k+G)^2+f\frac{\omega_p^2}{c^2}\right]-i\frac{\gamma}{c}(k+G)^2\right)B(k|G)-\mu\frac{\omega_p^2}{c^2}{\sum_{G'}}'\,f\frac{\sin(|G-G'|R)}{(|G-G'|R)}B(k|G')=0, \tag{2.10}$$

which has the form of a generalized eigenvalue problem for a complex matrix. For sufficiently small values of the filling fraction, we can treat the nondiagonal terms in Eq. (2.10) as a perturbation, and we proceed in two steps as follows: we first seek the zero-order eigenvalues given by the solutions of the equations which correspond to the diagonal terms of the matrix equation (2.10) for each value of the reciprocal-lattice vector G used in the expansions given by Eqs. (2.2) and (2.7). In the second step we substitute the zero-order eigenvalues and the nondiagonal terms in Eq. (2.10), $-\mu f(\omega_p^2/c^2)\sin(|G-G'|R)/(|G-G'|R)$, into a standard first-order perturbation formula to calculate corrected eigenvalues.

We can write the complex variable μ in the form $\mu=\omega_R/c+i\omega_I/c$, where ω_R represents the real part of the frequency, and ω_I determines the lifetime τ of the wave according to the definition

$$\frac{1}{\tau}=-2\omega_I. \tag{2.11}$$

It is obvious that, in terms of ω_R/c and ω_I/c, Eq. (2.10) can be replaced by a pair of coupled equations for the real and imaginary parts of the complex variable μ for each value of G in the form

$$\omega_R^3-\omega_R[3\omega_I^2+2\omega_I\gamma+c^2(k+G)^2+f\omega_p^2]=0, \tag{2.12a}$$

$$\omega_I^3+\gamma\omega_I^2-\omega_I[3\omega_R^2-c^2(k+G)^2-f\omega_p^2]-\gamma[\omega_R^2-c^2(k+G)^2]=0. \tag{2.12b}$$

If we assume $\omega_R\neq 0$, then we can eliminate ω_R by substituting ω_R^2 given by

$$\omega_R^2=3\omega_I^2+2\omega_I\gamma+c^2(k+G)^2+f\omega_p^2 \tag{2.13}$$

into Eq. (2.12b), which gives

$$\omega_I^3+\omega_I^2\gamma+\omega_I\tfrac{1}{4}[c^2(k+G)^2+f\omega_p^2+\gamma^2]+\frac{\gamma}{8}\omega_p^2f=0. \tag{2.14}$$

The latter equation can be transformed into the form

$$\omega_Z^3+p\omega_Z+q=0 \tag{2.15}$$

by the use of the substitution $\omega_Z=\omega_I+\gamma/3$, where

$$p=\tfrac{1}{4}[c^2(k+G)^2+f\omega_p^2]-\frac{\gamma^2}{12}, \tag{2.16a}$$

$$q=\frac{2\gamma^3}{27}-\frac{\gamma}{12}[c^2(k+G)^2+f\omega_p^2+\gamma^2]+\frac{\gamma}{8}\omega_p^2f. \tag{2.16b}$$

Then we retain the roots of Eqs. (2.12), which yield positive values for both ω_R and τ for each EM mode. Finally, the substitution of the zero-order eigenvalues given by the roots $\mu_G^{(0)}$ of Eq. (2.12) and the nondiagonal terms of Eq. (2.10) into the standard first-order perturbation formula gives the corrected eigenvalues μ_G ,

$$\mu_G=\mu_G^{(0)}+\sum_{G'}\frac{Q_{GG'}Q_{G'G}}{\mu_G^{(0)}-\mu_{G'}^{(0)}}, \tag{2.17}$$

where $\mu_G^{(0)}=\omega_R/c+i\omega_I/c$ are the zero-order eigenvalues for each value of the reciprocal-lattice vectors G, and $Q_{GG'}$ are the nondiagonal elements

$$Q_{GG'}=-\mu_G^{(0)}f\frac{\omega_p^2}{c^2}\frac{\sin(|G-G'|R)}{(|G-G'|R)}. \tag{2.18}$$

B. Construction of an equivalent matrix

The linearization technique is a standard method which transforms the nonlinear matrix equation into a linear form by construction of an equivalent matrix whose dimension is the number of plane waves used multiplied by the order of the polynomial eigenvalue problem.[36,37] We employ this

method to calculate the photonic band structures of the electromagnetic waves propagating through the one-dimensional system described in the Sec. II A. We first rewrite Eq. (2.10) in the form

$$\mu^3 \overleftrightarrow{I} - \mu^2 \overleftrightarrow{P} - \mu \overleftrightarrow{Q} - \overleftrightarrow{R} = 0, \tag{2.19}$$

where the elements of the $NG \times NG$ matrices $\overleftrightarrow{P}, \overleftrightarrow{Q}$, and $\overleftrightarrow{R}$ are given by

$$\overleftrightarrow{P}(G|G') = -i\frac{\gamma}{c}\delta_{G,G'} \tag{2.20a}$$

$$\overleftrightarrow{Q}(G|G') = \delta_{G,G'}\left[(k+G)^2 + f\frac{\omega_p^2}{c^2}\right] + f\frac{\omega_p^2}{c^2}\frac{\sin(|G-G'|R)}{(|G-G'|R)} \tag{2.20b}$$

$$\overleftrightarrow{R}(G|G') = i\frac{\gamma}{c}\delta_{G,G'}(k+G)^2, \tag{2.20c}$$

and NG is the number of the plane waves used in the expansions of $\epsilon(x_1|\omega)$ and $E(x_1|\omega)$ given by Eqs. (2.2) and (2.7), respectively. Equation (2.19) represents a nonlinear problem of the third order, which can be reformulated as a linear problem in $3NG$ dimensions, where the equivalent matrix $\overleftrightarrow{W}$ has the form

$$\overleftrightarrow{W}(G,G') = \begin{bmatrix} 0 & \overleftrightarrow{I} & 0 \\ 0 & 0 & \overleftrightarrow{I} \\ \overleftrightarrow{R} & \overleftrightarrow{Q} & \overleftrightarrow{P} \end{bmatrix}. \tag{2.21}$$

The complete solution of Eq. (2.19) is obtained by solving for the eigenvalues of $\overleftrightarrow{W}$ by the diagonalization of this complex, non-Hermitian matrix. We can write the eigenvalues, which are complex, in the form $\mu = \omega_R/c + i\omega_I/c$, where ω_R represents the real part of the frequency, and ω_I determines the lifetime τ of the wave according to the definition given by Eq. (2.11). Since the eigenvalues obtained by diagonalization yield a general solution, we have to discard the solutions which correspond to unphysical modes, i.e., those with a negative real part ω_R/c and with a positive imaginary part ω_I yielding a negative lifetime. This technique is an accurate method which yields results that can be used as benchmarks against which the photonic band structures obtained by our plane-wave approach can be compared. The linearization technique, however, requires the diagonalization of a high-dimensional matrix of order $3NG$, which makes the evaluation of the eigenvalues highly computer-intensive.

C. Transfer-matrix method

We consider the periodic structure that underlies the calculations of 1D photonic band structures—an infinite, alternating array of slabs each of thickness a, each of which is separated from its neighbors by vacuum layers of thickness b. The dispersion relation for electromagnetic waves incident normally on this structure has the form[38]

$$\cos k(a+b) = \cos\sqrt{\epsilon(\omega)}\frac{\omega a}{c}\cos\frac{\omega b}{c} - \frac{1}{2}\left(\sqrt{\epsilon(\omega)} + \frac{1}{\sqrt{\epsilon(\omega)}}\right) \times \sin\sqrt{\epsilon(\omega)}\frac{\omega a}{c}\sin\frac{\omega b}{c}. \tag{2.22}$$

Let us now consider the specific forms of the right-hand side of the latter equation corresponding to the dielectric functions used to describe the components. In the absence of dissipation the metallic components are characterized by a real, frequency-dependent dielectric function that has the simple free-electron metal form

$$\epsilon(\omega) = 1 - \omega_p^2/\omega^2. \tag{2.23}$$

Since the dielectric function given by Eq. (2.23) is negative in the frequency range $\omega < \omega_p$, its square root is pure imaginary, and the right-hand side of Eq. (2.22) is real as well as the resulting dispersion relation, which has the form

$$\cos k(a+b) = \cosh|\epsilon(\omega)|^{1/2}\frac{\omega a}{c}\cos\frac{\omega b}{c} + \frac{1}{2}\left(|\epsilon(\omega)|^{1/2} - \frac{1}{|\epsilon(\omega)|^{1/2}}\right) \times \sinh|\epsilon(\omega)|^{1/2}\frac{\omega a}{c}\sin\frac{\omega b}{c}. \tag{2.24}$$

If dissipation is introduced into the metallic components through the use of the dielectric function given by Eq. (1.1), the right-hand side of the Eq. (2.22) is also complex, and the dispersion relation takes the form

$$\cos K(a+b) = f_1(\omega) + i f_2(\omega), \tag{2.25}$$

where $K = k_R + ik_I$ represents a complex wave vector, and $f_1(\omega)$ and $f_2(\omega)$ represent the real and imaginary parts of the right-hand side of Eq. (2.22). We can write $f_1(\omega)$ and $f_2(\omega)$ explicitly in the forms

$$f_1(\omega) = \cos\left(n_R\frac{\omega a}{c}\right)\cosh\left(n_I\frac{\omega a}{c}\right)\cos\frac{\omega b}{c} - \frac{1}{2}\left[\xi^R(\omega)\sin\left(n_R\frac{\omega a}{c}\right)\cosh\left(n_I\frac{\omega a}{c}\right) + \xi^I(\omega)\sinh\left(n_I\frac{\omega a}{c}\right)\cos\left(n_R\frac{\omega a}{c}\right)\sin\frac{\omega b}{c}\right], \tag{2.26a}$$

$$f_2(\omega) = -\sin\left(n_R\frac{\omega a}{c}\right)\sinh\left(n_I\frac{\omega a}{c}\right)\cos\frac{\omega b}{c} - \frac{1}{2}\left[\xi^R(\omega)\sinh\left(n_I\frac{\omega a}{c}\right)\cos\left(n_R\frac{\omega a}{c}\right) + \xi^I(\omega)\sin\left(n_R\frac{\omega a}{c}\right)\cosh\left(n_I\frac{\omega a}{c}\right)\sin\frac{\omega b}{c}\right], \tag{2.26b}$$

where

$$\sqrt{\epsilon(\omega)} = n_R + i n_I \tag{2.27}$$

and

$$\xi(\omega) = \xi^R(\omega) + i\xi^I(\omega) \equiv \sqrt{\epsilon(\omega)} + \frac{1}{\sqrt{\epsilon(\omega)}}. \tag{2.28}$$

The real part of the complex wave vector K corresponds to the wave number k, while the imaginary part determines the absorption coefficient α as the inverse of the attenuation length l according the following definition:

$$\frac{1}{l} = \alpha = 2k_I. \tag{2.29}$$

The solutions of Eqs. (2.22), (2.24), and (2.25) are found by seeking the frequencies ω which for a given wave vector k satisfy these equations. The resulting dispersion curves can be displayed directly by plotting the right-hand side of Eq. (2.22) as a function of frequency when the dielectric function is real and frequency dependent. When the dielectric function $\epsilon(\omega)$ is complex we also have to consider the complex nature of the wave vector K in Eq. (2.25), and we obtain a set of equations which allow obtaining each of its components. Consequently, the real part of the photonic band structure can be found by seeking the frequencies ω which satisfy for given wave number k_R the following equation:

$$\cos k_R(a+b) = f_1(\omega)\left[\frac{f_2^2(\omega)}{\sin^2 k_R(a+b)} + 1\right]^{-1/2}. \tag{2.30}$$

Equation (2.25) was solved numerically to determine a complex photonic band structure, which, besides the dispersion curves $\omega = \omega(k)$, also yields the absorption coefficient α of the corresponding mode. While we use the resulting dispersion curves as the benchmark against which we compare the real part of the photonic band structure obtained by the perturbative plane-wave method (PWM) approach described in Sec. II A, the absorption coefficients represent a complementary characteristic to that of the mode lifetime obtained by the PWM approach.

III. TWO-DIMENSIONAL SYSTEM-METALLIC RODS IN THE PRESENCE OF DISSIPATION

The method outlined in Sec. II A can be readily generalized to two dimensions. Specifically, we consider a system consisting of an array of infinitely long metallic cylinders of circular cross section surrounded by vacuum, whose intersections with a perpendicular plane form a simple square lattice. We assume that the axes of the cylinders are parallel to the x_3 axis, and the positions of the sites of this lattice are given by the vectors

$$\mathbf{x}_\parallel(l) = l_1\mathbf{a}_1 + l_2\mathbf{a}_2, \tag{3.1}$$

where $\mathbf{a}_1$ and $\mathbf{a}_2$ are the two, noncolinear, primitive translation vectors of the lattice, while l_1 and l_2 are arbitrary integers that we denote collectively by l. The area a_c of a primitive unit cell of this lattice is given by

$$a_c = |\mathbf{a}_1 \times \mathbf{a}_2|. \tag{3.2}$$

The lattice reciprocal to the direct lattice whose points are defined by Eq. (3.1) is defined by the translation vectors

$$\mathbf{G}_\parallel(h) = h_1\mathbf{b}_1 + h_2\mathbf{b}_2, \tag{3.3}$$

where $\mathbf{b}_1$ and $\mathbf{b}_2$ are the primitive translation vectors of the reciprocal lattice, and h_1 and h_2 are arbitrary integers which we denote collectively by h. The dielectric function of this system, $\epsilon(\mathbf{x}_\parallel|\omega)$, is a position-dependent, periodic function of $\mathbf{x}_\parallel$ with the periodicity of the Bravais lattice defined by Eq. (3.1),

$$\epsilon[\mathbf{x}_\parallel + \mathbf{x}_\parallel(l)|\omega] = \epsilon(\mathbf{x}_\parallel|\omega). \tag{3.4}$$

It can therefore be expanded into a two-dimensional Fourier series according to

$$\epsilon(\mathbf{x}_\parallel|\omega) = \sum_{\mathbf{G}_\parallel} \hat{\epsilon}(\mathbf{G}_\parallel) e^{i\mathbf{G}_\parallel\cdot\mathbf{x}_\parallel}. \tag{3.5}$$

In the particular case of cylinders characterized by the dielectric function (1.1), whose cross section is a circle of radius R, for the Fourier coefficients $\hat{\epsilon}(\mathbf{G}_\parallel)$ we obtain

$$\hat{\epsilon}(\mathbf{G}_\parallel) = 1 - f\frac{\omega_p^2}{\omega(\omega + i\gamma)}, \quad \mathbf{G}_\parallel = \mathbf{0} \tag{3.6a}$$

$$= -f\frac{\omega_p^2}{\omega(\omega+i\gamma)}\frac{2J_1(G_\parallel R)}{(G_\parallel R)}, \quad \mathbf{G}_\parallel \neq \mathbf{0}. \tag{3.6b}$$

Here $f = \pi R^2/a_c$ is the filling fraction, i.e., the fraction of the volume occupied by the rods, and $J_1(x)$ is a Bessel function.

The inverse dielectric function $\epsilon(\mathbf{x}_\parallel|\omega)^{-1}$ can also be expanded in a two-dimensional Fourier series according to

$$\frac{1}{\epsilon(\mathbf{x}_\parallel|\omega)} = \sum_{\mathbf{G}_\parallel} \hat{\kappa}(\mathbf{G}_\parallel) e^{i\mathbf{G}_\parallel\cdot\mathbf{x}_\parallel}. \tag{3.7}$$

The Fourier coefficients $\hat{\kappa}(\mathbf{G}_\parallel)$ in the case of rods assumed to have a circular cross section of radius R are then given by

$$\hat{\kappa}(\mathbf{G}_\parallel) = 1 + f\frac{\omega_p^2}{\omega^2 - \omega_p^2 + i\gamma\omega}, \quad \mathbf{G}_\parallel = \mathbf{0} \tag{3.8a}$$

$$= \frac{\omega_p^2}{\omega^2 - \omega_p^2 + i\gamma\omega} f\frac{2J_1(G_\parallel R)}{(G_\parallel R)}, \quad \mathbf{G}_\parallel \neq \mathbf{0}. \tag{3.8b}$$

We now apply these results to the determination of the photonic band structures of E- and H-polarized electromagnetic waves in the system described by this dielectric function.

A. E polarization

1. Reduction to a set of simultaneous nonlinear equations

In the case of E polarization, we seek solutions of the Maxwell equations which have the forms

$$\mathbf{E}(\mathbf{x};t)=(0,0,E_3(\mathbf{x}_\parallel|\omega))\exp(-i\omega t), \tag{3.9a}$$

$$\mathbf{H}(\mathbf{x};t)=(H_1(\mathbf{x}_\parallel|\omega),H_2(\mathbf{x}_\parallel|\omega),0)\exp(-i\omega t). \tag{3.9b}$$

The Maxwell curl equations for the three nonzero field components are

$$\frac{\partial H_2}{\partial x_1}-\frac{\partial H_1}{\partial x_2}=-i\frac{\omega}{c}D_3=-i\frac{\omega}{c}\epsilon(\mathbf{x}_\parallel|\omega)E_3, \tag{3.10a}$$

$$\frac{\partial E_3}{\partial x_1}=-i\frac{\omega}{c}H_2, \tag{3.10b}$$

$$\frac{\partial E_3}{\partial x_2}=i\frac{\omega}{c}H_1. \tag{3.10c}$$

When we eliminate H_1 and H_2 from these equations, we obtain, as the equation satisfied by E_3,

$$\left(\frac{\partial^2}{\partial x_1^2}+\frac{\partial^2}{\partial x_2^2}\right)E_3+\epsilon(\mathbf{x}_\parallel|\omega)\frac{\omega^2}{c^2}E_3=0. \tag{3.11}$$

To solve Eq. (3.11) we use the expansion (3.5), and write $E_3(\mathbf{x}_\parallel|\omega)$ in the form

$$E_3(\mathbf{x}_\parallel|\omega)=\sum_{\mathbf{G}_\parallel}B(\mathbf{k}_\parallel|\mathbf{G}_\parallel)e^{i(\mathbf{k}_\parallel+\mathbf{G}_\parallel)\cdot\mathbf{x}_\parallel}, \tag{3.12}$$

where $\mathbf{k}_\parallel=(k_1,k_2,0)$ is the two-dimensional wave vector of the wave. When these expansions are substituted into Eq. (3.11), we obtain, as the equation satisfied by the coefficients $\{B(\mathbf{k}_\parallel|\mathbf{G}_\parallel)\}$,

$$(\mathbf{k}_\parallel+\mathbf{G}_\parallel)^2B(\mathbf{k}_\parallel|\mathbf{G}_\parallel)=\frac{\omega^2}{c^2}\hat{\epsilon}(\mathbf{0})B(\mathbf{k}_\parallel|\mathbf{G}_\parallel)+\frac{\omega^2}{c^2}{\sum_{\mathbf{G}_\parallel}}'\,\hat{\epsilon}(\mathbf{G}_\parallel-\mathbf{G}_\parallel')B(\mathbf{k}_\parallel|\mathbf{G}_\parallel'), \tag{3.13}$$

where the prime on the sum over $\mathbf{G}_\parallel'$ indicates that the term with $\mathbf{G}_\parallel'=\mathbf{G}_\parallel$ is omitted. We now use the definition of μ given by Eq. (2.9), and the result for $\hat{\epsilon}(\mathbf{G}_\parallel)$ given by Eqs. (3.6), to transform Eq. (3.13) into

$$\left(\mu^3+i\frac{\gamma}{c}\mu^2-\mu\left[(\mathbf{k}_\parallel+\mathbf{G}_\parallel)^2+f\frac{\omega_p^2}{c^2}\right]-i\frac{\gamma}{c}(\mathbf{k}_\parallel+\mathbf{G}_\parallel)^2\right)B(\mathbf{k}_\parallel|\mathbf{G}_\parallel)-\mu\frac{\omega_p^2}{c^2}{\sum_{\mathbf{G}_\parallel'}}\,f\frac{2J_1(|\mathbf{G}_\parallel-\mathbf{G}_\parallel'|R)}{(|\mathbf{G}_\parallel-\mathbf{G}_\parallel'|R)}B(\mathbf{k}_\parallel|\mathbf{G}_\parallel')=0, \tag{3.14}$$

which has the form of a generalized eigenvalue problem for a complex matrix. To solve this matrix equation for sufficiently small values of the filling fraction, we proceed according to the method described in Sec. II: We first solve separately the equations which correspond to the diagonal terms of the matrix equation (3.14) to obtain the zero-order eigenvalues $\mu_{G_\parallel}^{(0)}$ for each value of the reciprocal-lattice vector $\mathbf{G}_\parallel$ used in the expansions given by Eqs. (3.5) and (3.12), and then substitute the nondiagonal terms of Eq. (3.14), $-\mu f(\omega_p^2/c^2)2J_1(|\mathbf{G}_\parallel-\mathbf{G}_\parallel'|R)/(\mathbf{G}_\parallel-\mathbf{G}_\parallel'|R)$ into the standard first-order perturbation formula to calculate the corrected eigenvalues.

2. Construction of an equivalent matrix

Now we apply the linearization scheme described in Sec. II B for the calculation of the photonic band structures of the electromagnetic waves propagating through the two-dimensional array of infinitely long dissipative metallic rods. We start from the nonlinear eigenvalue problem given by Eq. (3.14), obtained by transforming Maxwell's equations for E-polarized electromagnetic waves by means of the plane-wave expansions (3.5) and (3.12). We rewrite Eq. (3.14) in the polynomial form

$$\mu^3\overleftrightarrow{I}-\mu^2\overleftrightarrow{P}-\mu\overleftrightarrow{Q}-\overleftrightarrow{R}=0, \tag{3.15}$$

where the elements of the $NG\times NG$ matrices $\overleftrightarrow{P},\overleftrightarrow{Q}$, and $\overleftrightarrow{R}$ are given by

$$\overleftrightarrow{P}(\mathbf{G}_\parallel|\mathbf{G}_\parallel')=-i\frac{\gamma}{c}\delta_{\mathbf{G}_\parallel,\mathbf{G}_\parallel'}, \tag{3.16a}$$

$$\overleftrightarrow{Q}(\mathbf{G}_\parallel|\mathbf{G}_\parallel')=\delta_{\mathbf{G}_\parallel,\mathbf{G}_\parallel'}\left[(\mathbf{k}_\parallel+\mathbf{G}_\parallel)^2+f\frac{\omega_p^2}{c^2}\right]+f\frac{\omega_p^2}{c^2}\frac{2J_1(|\mathbf{G}_\parallel-\mathbf{G}_\parallel'|R)}{(|\mathbf{G}_\parallel-\mathbf{G}_\parallel'|R)}, \tag{3.16b}$$

$$\overleftrightarrow{R}(\mathbf{G}_\parallel|\mathbf{G}_\parallel')=i\frac{\gamma}{c}\delta_{\mathbf{G}_\parallel,\mathbf{G}_\parallel'}(\mathbf{k}_\parallel+\mathbf{G}_\parallel)^2, \tag{3.16c}$$

and NG is the number of plane waves used in the expansions of $\epsilon(\mathbf{x}_\parallel|\omega)$ and $E_3(\mathbf{x}_\parallel|\omega)$ given by Eqs. (3.5) and (3.12), respectively. The nonlinear eigenvalue problem given by Eq. (3.15) can be transformed into a linear problem in $3NG$ dimensions by the construction of a matrix $\overleftrightarrow{W}$ given by

$$\overleftrightarrow{W}(\mathbf{G}_\parallel|\mathbf{G}'_\parallel)=\begin{bmatrix} \mathbf{0} & \overleftrightarrow{I} & \mathbf{0} \\ \mathbf{0} & \mathbf{0} & \overleftrightarrow{I} \\ \overleftrightarrow{R} & \overleftrightarrow{Q} & \overleftrightarrow{P} \end{bmatrix}. \tag{3.17}$$

The solution of Eq. (3.14) is reduced to the diagonalization of the complex, non-Hermitian matrix $\overleftrightarrow{W}$, which yields complex eigenvalues. We select the solutions with a positive real component and a negative imaginary component, which correspond to the physical modes that can be expressed in the form $\mu=\omega_R/c+i\omega_I/c$ according the definition introduced in Sec. II B. The results obtained by this approach provide standard solutions which can be directly compared to those obtained by our perturbative plane wave method.

B. *H* polarization

1. Reduction to a set of simultaneous nonlinear equations

In the case of H polarization, we seek solutions of the Maxwell equations which have the forms

$$\mathbf{H}(\mathbf{x};t)=(0,0,H_3(\mathbf{x}_\parallel|\omega))\exp(-i\omega t), \tag{3.18a}$$

$$\mathbf{E}(\mathbf{x};t)=(E_1(\mathbf{x}_\parallel|\omega),E_2(\mathbf{x}_\parallel|\omega),0)\exp(-i\omega t). \tag{3.18b}$$

The Maxwell curl equations in this case are

$$\frac{\partial E_2}{\partial x_1}-\frac{\partial E_1}{\partial x_2}=i\frac{\omega}{c}H_3, \tag{3.19a}$$

$$\frac{\partial H_3}{\partial x_1}=i\frac{\omega}{c}D_2=i\frac{\omega}{c}\epsilon(\mathbf{x}_\parallel|\omega)E_2, \tag{3.19b}$$

$$\frac{\partial H_3}{\partial x_2}=-i\frac{\omega}{c}D_1=-i\frac{\omega}{c}\epsilon(\mathbf{x}_\parallel|\omega)E_1. \tag{3.19c}$$

When we eliminate E_1 and E_2 from these equations, we obtain the equation satisfied by H_3, which we write in the form

$$\frac{\partial}{\partial x_1}\left(\frac{1}{\epsilon(\mathbf{x}_\parallel|\omega)}\frac{\partial H_3}{\partial x_1}\right)+\frac{\partial}{\partial x_2}\left(\frac{1}{\epsilon(\mathbf{x}_\parallel|\omega)}\frac{\partial H_3}{\partial x_2}\right)+\frac{\omega^2}{c^2}H_3=0. \tag{3.20}$$

To solve this equation, we expand $H_3(\mathbf{x}_\parallel)$ according to

$$H_3(\mathbf{x}_\parallel|\omega)=\sum_{\mathbf{G}_\parallel}A(\mathbf{k}_\parallel|\mathbf{G}_\parallel)e^{i(\mathbf{k}_\parallel+\mathbf{G}_\parallel)\cdot\mathbf{x}_\parallel}. \tag{3.21}$$

When we substitute the latter expansion together with the expansion of $\epsilon^{-1}(\mathbf{x}_\parallel|\omega)$ given by Eq. (3.7) into Eq. (3.20), we obtain as the equation satisfied by the coefficients $\{A(\mathbf{k}_\parallel|\mathbf{G}_\parallel)\}$,

$$\sum_{\mathbf{G}'_\parallel}(\mathbf{k}_\parallel+\mathbf{G}_\parallel)\cdot(\mathbf{k}_\parallel+\mathbf{G}'_\parallel)\hat{\kappa}(\mathbf{G}_\parallel-\mathbf{G}'_\parallel)A(\mathbf{k}_\parallel|\mathbf{G}'_\parallel)=\frac{\omega^2}{c^2}A(\mathbf{k}_\parallel|\mathbf{G}_\parallel). \tag{3.22}$$

Now we use the definition of μ given by Eq. (2.9) and the Fourier coefficients $\{\hat{\kappa}(\mathbf{G}_\parallel)\}$ given by Eqs. (3.8) in Eq. (3.22), which transform the latter into

$$\begin{aligned}&\left(\mu^4+i\frac{\gamma}{c}\mu^3-\mu^2\left[(\mathbf{k}_\parallel+\mathbf{G}_\parallel)^2+\frac{\omega_p^2}{c^2}\right]-i\mu\frac{\gamma}{c}(\mathbf{k}_\parallel+\mathbf{G}_\parallel)^2\right.\\&\left.+(1-f)\frac{\omega_p^2}{c^2}(\mathbf{k}_\parallel+\mathbf{G}_\parallel)^2\right)A(\mathbf{k}_\parallel|\mathbf{G}_\parallel)\\&-f\frac{\omega_p^2}{c^2}\sum_{\mathbf{G}'_\parallel}\frac{2J_1(|\mathbf{G}_\parallel-\mathbf{G}'_\parallel|R)}{(|\mathbf{G}_\parallel-\mathbf{G}'_\parallel|R)}\\&\times(\mathbf{k}_\parallel+\mathbf{G}_\parallel)\cdot(\mathbf{k}_\parallel+\mathbf{G}'_\parallel)A(\mathbf{k}_\parallel|\mathbf{G}'_\parallel)=0,\end{aligned} \tag{3.23}$$

which has the form of a generalized eigenvalue problem for a complex matrix. To solve this matrix equation, we use the same approach as we applied in the case of E polarization: we first solve the equations which correspond to the diagonal terms of the matrix Eq. (3.23) to obtain the zero-order eigenvalues $\mu^{(0)}_{G_\parallel}$ for each value of the reciprocal-lattice vector $\mathbf{G}_\parallel$ used in the expansions given by Eqs. (3.7) and (3.21), and then we use perturbation theory to obtain the corrected eigenvalues by taking the nondiagonal terms given by the last term in the latter equation, $-f(\omega_p^2/c^2)(\mathbf{k}_\parallel+\mathbf{G}_\parallel)\cdot(\mathbf{k}_\parallel+\mathbf{G}'_\parallel)2J_1(|\mathbf{G}_\parallel-\mathbf{G}'_\parallel|R)/(|\mathbf{G}_\parallel-\mathbf{G}'_\parallel|R)$, as a perturbation.

The diagonal terms of the matrix Eq. (3.23) can be rewritten as a pair of coupled nonlinear equations in terms of the components ω_R/c and ω_I/c of the complex variable μ given by Eq. (2.9) for each $\mathbf{G}_\parallel$:

$$\begin{aligned}&\omega_R^4-\omega_R^2[6\omega_I^2+3\omega_I\gamma+c^2(\mathbf{k}_\parallel+\mathbf{G}_\parallel)^2+\omega_p^2]+\omega_I^4+\gamma\omega_I^3\\&+\omega_I^2[c^2(\mathbf{k}_\parallel+\mathbf{G}_\parallel)^2+\omega_p^2]+\omega_I\gamma c^2(\mathbf{k}_\parallel+\mathbf{G}_\parallel)^2\\&+(1-f)\omega_p^2c^2(\mathbf{k}_\parallel+\mathbf{G}_\parallel)^2=0,\end{aligned} \tag{3.24a}$$

$$\begin{aligned}&\omega_I^3+\frac{3\gamma}{4}\omega_I^2+\omega_I\{0.5[c^2(\mathbf{k}_\parallel+\mathbf{G}_\parallel)^2+\omega_p^2]-\omega_R^2\}-\omega_R^2\frac{\gamma}{4}\\&+\frac{\gamma}{4}c^2(\mathbf{k}_\parallel+\mathbf{G}_\parallel)^2=0.\end{aligned} \tag{3.24b}$$

We solved these coupled nonlinear equations numerically for each vector $\mathbf{G}_\parallel$ used in the expansions given by Eqs. (3.7) and (3.21), by using the computational procedure from MATHEMATICA,[39] and retained only the solutions of physical interest, i.e., those for which $\mathrm{Re}[\mu^{(0)}_{G_\parallel}(\mathbf{k}_\parallel)]\geqslant 0$ and $\mathrm{Im}[\mu^{(0)}_{G_\parallel}(\mathbf{k}_\parallel)]\leqslant 0$.

2. Construction of an equivalent matrix

In this section we apply the linearization technique described in Sec. III A 2 for calculating the photonic band structure of H-polarized electromagnetic waves propagating through the two-dimensional periodic system considered in Sec. III. In this case Maxwell's equations for the magnetic vector are transformed by the plane wave expansions (3.7) and (3.21) into the generalized nonlinear eigenvalue problem given by Eq. (3.23), which can be rewritten in the polynomial form

$$\mu^4\overleftrightarrow{I}-\mu^3\overleftrightarrow{R}-\mu^2\overleftrightarrow{S}-\mu\overleftrightarrow{T}-\overleftrightarrow{U}=0, \tag{3.25}$$

where the elements of the $NG\times NG$ matrices $\overleftrightarrow{R}$, $\overleftrightarrow{S}$, $\overleftrightarrow{T}$, and $\overleftrightarrow{U}$ are given by

$$\overleftrightarrow{R}(\mathbf{G}_\parallel|\mathbf{G}'_\parallel)=-i\frac{\gamma}{c}\delta_{\mathbf{G}_\parallel,\mathbf{G}'_\parallel}, \tag{3.26a}$$

$$\overleftrightarrow{S}(\mathbf{G}_\parallel|\mathbf{G}'_\parallel)=\delta_{\mathbf{G}_\parallel,\mathbf{G}'_\parallel}\left[(\mathbf{k}_\parallel+\mathbf{G}_\parallel)^2+\frac{\omega_p^2}{c^2}\right], \tag{3.26b}$$

$$\overleftrightarrow{T}(\mathbf{G}_\parallel|\mathbf{G}'_\parallel)=i\frac{\gamma}{c}\delta_{\mathbf{G}_\parallel,\mathbf{G}'_\parallel}(\mathbf{k}_\parallel+\mathbf{G}_\parallel)^2, \tag{3.26c}$$

$$\overleftrightarrow{U}(\mathbf{G}_\parallel|\mathbf{G}'_\parallel)=\delta_{\mathbf{G}_\parallel,\mathbf{G}'_\parallel}\frac{\omega_p^2}{c^2}(f-1)(\mathbf{k}_\parallel+\mathbf{G}_\parallel)^2 + f\frac{\omega_p^2}{c^2}\frac{2J_1(|\mathbf{G}_\parallel-\mathbf{G}'_\parallel|R)}{(|\mathbf{G}_\parallel-\mathbf{G}'_\parallel|R)}(\mathbf{k}_\parallel+\mathbf{G}_\parallel)\cdot(\mathbf{k}_\parallel+\mathbf{G}'_\parallel), \tag{3.26d}$$

and NG is the number of the plane waves used in expansions of $\epsilon^{-1}(\mathbf{x}_\parallel|\omega)$ and $H_3(\mathbf{x}_\parallel|\omega)$ given by Eqs. (3.7) and (3.21), respectively. The nonlinear eigenvalue problem given by Eq. (3.25) can be transformed into a linear problem in $4NG$ dimensions by the construction of a matrix $\overleftrightarrow{V}$ given by

$$\overleftrightarrow{V}(\mathbf{G}_\parallel|\mathbf{G}'_\parallel)=\begin{bmatrix}\mathbf{0} & \overleftrightarrow{I} & \mathbf{0} & \mathbf{0}\\ \mathbf{0} & \mathbf{0} & \overleftrightarrow{I} & \mathbf{0}\\ \mathbf{0} & \mathbf{0} & \mathbf{0} & \overleftrightarrow{I}\\ \overleftrightarrow{U} & \overleftrightarrow{T} & \overleftrightarrow{S} & \overleftrightarrow{R}\end{bmatrix}. \tag{3.27}$$

The solution of Eq. (3.25) is reduced to the diagonalization of the complex, non-Hermitian matrix $\overleftrightarrow{V}$, which yields complex eigenvalues. We select the solutions with a positive real component and a negative imaginary component, which correspond to the physical modes that can be expressed in the form $\mu=\omega_R/c+i\omega_I/c$ according the definition introduced in Sec. II B. The results obtained by the linearization technique are used as the standard solution which allows direct comparison to the results obtained by our perturbative plane-wave method.

IV. RESULTS

A. 1D systems

We first consider the results obtained by the transfer-matrix method for a structure consisting of metallic components characterized by the complex dielectric function $\epsilon(\omega)$ given by Eq. (1.1), which can be written explicitly as

$$\epsilon(\omega)=\epsilon_R^m(\omega)+i\epsilon_I^m(\omega), \tag{4.1}$$

where

$$\epsilon_R^m(\omega)=1-\frac{\omega_p^2}{\omega^2+\gamma^2},\quad \epsilon_I^m(\omega)=\frac{\gamma\omega_p^2}{\omega(\omega^2+\gamma^2)}. \tag{4.2}$$

A typical value of the plasma frequency of the conduction electrons in metals, which usually lies in the ultraviolet region of the optical spectrum, is $\omega_p\sim10^{15}\ \mathrm{s}^{-1}$, while a typical value of the electron relaxation time is $\tau_e\sim10^{-13}$ s. Therefore, we used the value of $\gamma=0.01\omega_p$ in obtaining these results. We took as a normalization condition $\omega_p a/2\pi c=1$, which determines the value of $\omega_R a/2\pi c$ at which the change in sign of $\epsilon_R^m(\omega)$ occurs when $\omega_R=\omega_P(1-\gamma^2/\omega_P^2)^{1/2}$.

In Fig. 1(a) we plot the six lowest-frequency bands which satisfy Eq. (2.27) for the filling fraction of the slabs $f=0.001$. The band structure for this value of the filling fraction is a slightly perturbed version of the dispersion relation for EM waves in vacuum. In Figs. 1(b) and 1(c) we depict the band structures which correspond to the filling fractions $f=0.01$ and 0.1, respectively. The dispersion curves exhibit the existence of a band gap below the lowest-energy band, and structural gaps between the higher energy bands—see Fig. 1(c). The presence of damping gives rise to an additional partial band below the lowest-frequency band for the filling fraction $f=0.1$, as is shown in Fig. 1(c). To analyze this effect we first compare the right-hand side of the dispersion relation (2.24) for metallic slabs characterized by the real, frequency-dependent dielectric function given by Eq. (2.23). The expression on the right-hand side of Eq. (2.24) exhibits harmonic behavior in the range of frequencies considered—see Fig. 2, and yields dispersion curves which correspond to the case without damping. If dissipation is introduced into the metallic components through the use of the complex dielectric function given by Eq. (1.1), the photonic band structure is negligibly changed over most of the frequency range, except in the vicinity of the pole at $\omega=0$, where the major change in the behavior of the function $f_1(\omega)$ given by Eq. (2.26a) occurs—see Fig. 3. As a result, an additional, lowest-frequency band, appears for small values of kd and vanishes at a finite value kd whose magnitude depends on the value of the damping constant γ used in the complex dielectric function $\epsilon(\omega)$ given by Eq. (1.1). The existence of this mode is primarily due to the singular behavior of the imaginary part $f_2(\omega)$ and the simultaneous, substantial, decrease of the real part $f_1(\omega)$ in the neighborhood of the pole at $\omega=0$.

In Fig. 4(a) we plot the absorption coefficient α associated with the six lowest-frequency bands on a logarithmic scale in the reduced zone scheme for a filling fraction $f=0.001$ in the standard reduced zone scheme. The absorption of the modes associated with the bands decreases with increasing wave number k, and displays a global maximum at the Γ point $k=0$, where the strongest absorption of the mode associated with the lowest band occurs. We have found that the absorption coefficient displays a remarkable feature—an asymmetric behavior near the Brillouin-zone boundaries. To demonstrate this effect we used the extended-zone scheme to display the absorption coefficient α on a logarithmic scale as a function of the wave number k for the filling fractions $f=0.001$, 0.01, and 0.1. The asymmetry of the absorption coefficient is represented by its decrease for electromagnetic waves with frequencies near the lower band edge at the Brillouin-zone boundary, and its significant increase for electromagnetic waves with frequencies in the neighborhood of the upper band edge at the Brillouin zone boundary. This effect becomes more pronounced when the filling fraction of the slabs is increased, as is seen in Fig.

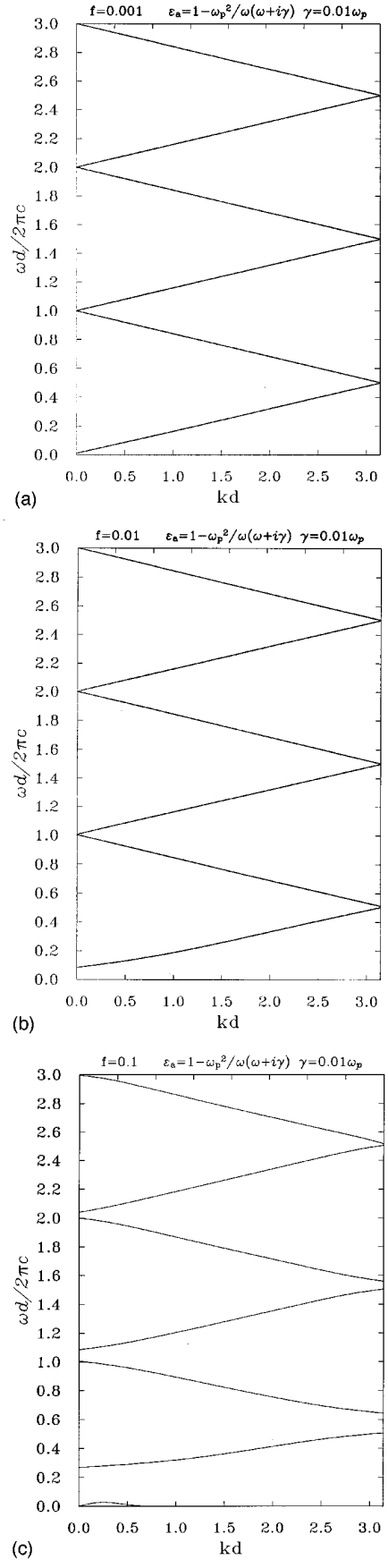

FIG. 1. The photonic band structure of a 1D lattice consisting of lossy metallic slabs in vacuum obtained by the transfer matrix method. E polarization: (a) $f=0.001$, (b) $f=0.01$, and (c) $f=0.1$.

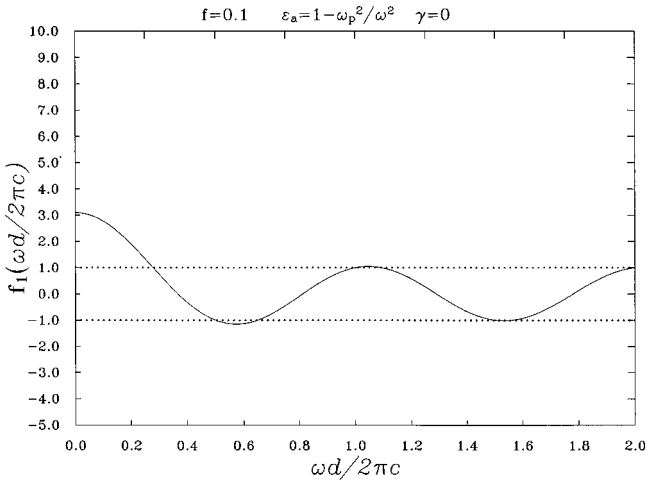

FIG. 2. The right-hand side of the dispersion relation given by Eq. (2.24) for a periodic system of metallic layers in which the effect of dissipation is not taken into account: $f=0.1$, $\gamma=0$, $0<\omega<2\omega_p$.

4(b), where the absorption coefficients for the three different values of the filling fractions are shown. One can see that, except at the Brillouin-zone boundaries, the absorption coefficient exhibits a monotonic dependence on the wave number, and has its maximum value for the lowest-frequency band at $kd=0$. The results shown in Fig. 4(b) also confirm the expected fact that the modes become increasingly absorbed with increasing value of the filling fraction.

We believe that the asymmetry in the absorption coefficient is due to the redistribution of the electromagnetic field at the top and the bottom of a gap. A solution near a band edge requires the use of degenerate perturbation theory, which yields two standing-wave solutions $\Psi_1(x) \propto \sin(\pi x/d)$, and $\Psi_2(x) \propto \cos(\pi x/d)$ for the photon wave function. Since the metal acts like a repulsive potential, the lower-frequency state corresponds to $\Psi_1(x)$, which peaks between the metal slabs. Consequently, the overlap of the EM field and the metal is minimized and the absorption is small. The upper state corresponds to the wave function

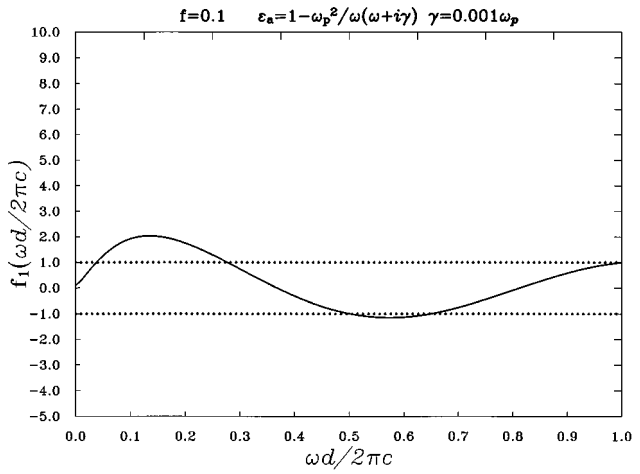

FIG. 3. The right-hand side of the dispersion relation given by Eq. (2.25) for a periodic system of metallic layers in presence of dissipation: $f=0.1$, $\gamma=0.001\omega_p$, $0<\omega<2\omega_p$.

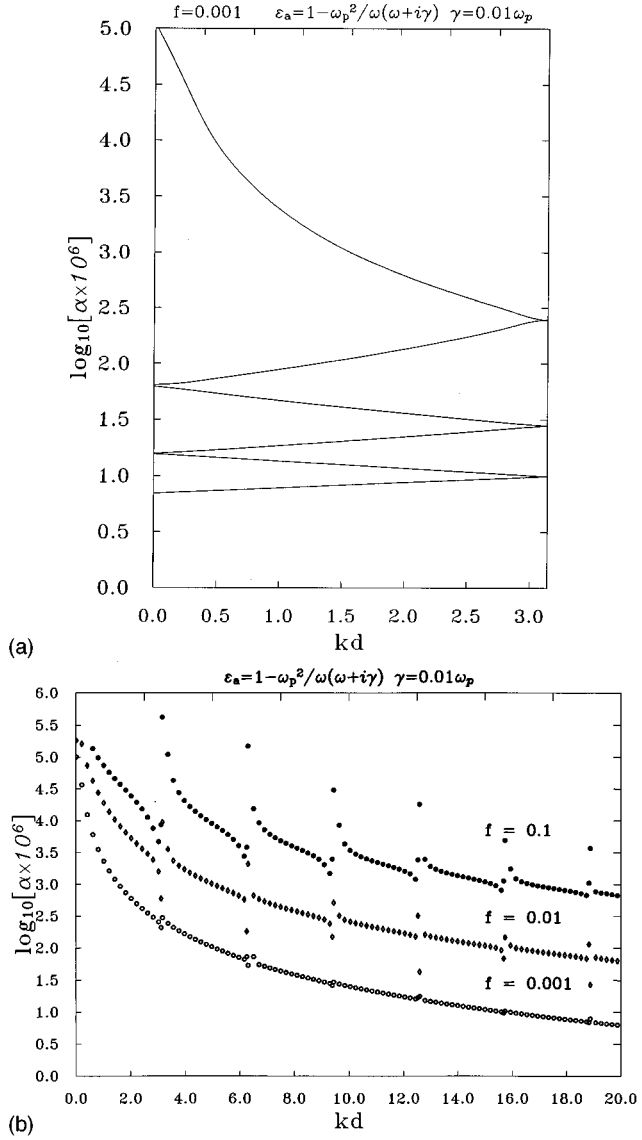

FIG. 4. The absorption coefficient of the modes associated with the photonic band structure of a 1D lattice consisting of lossy metallic slabs in vacuum displayed in reduced zone scheme: (a) $f=0.001$; extended-zone scheme: (b) $f=0.001$ (○○○○), $f=0.01$ (◇ ◇ ◇ ◇), and $f=0.1$ (●●●●).

$\Psi_2(x)$, which has nodes between the slabs. Therefore the overlap between the metal and the field is maximized, and the absorption is greater.

We now turn to the results obtained by the perturbative plane-wave method described in Sec. II A for a structure of metallic layers. In Figs. 5(a) and 5(b) we present the dispersion curves which include the five lowest-frequency bands for a 1D lattice formed by the metallic slabs in vacuum when the filling fraction of the slabs is $f=0.001$ and 0.01, respectively. A total of 91 plane waves was used in obtaining these results. The results presented are in good agreement with the results obtained by the transfer-matrix method. The dispersion curves exhibit the existence of a band gap below the lowest band at the Γ point, whose width increases as the filling fraction is increased. They do not reveal the existence of an additional band below the lowest-frequency band, as found by the transfer-matrix method.

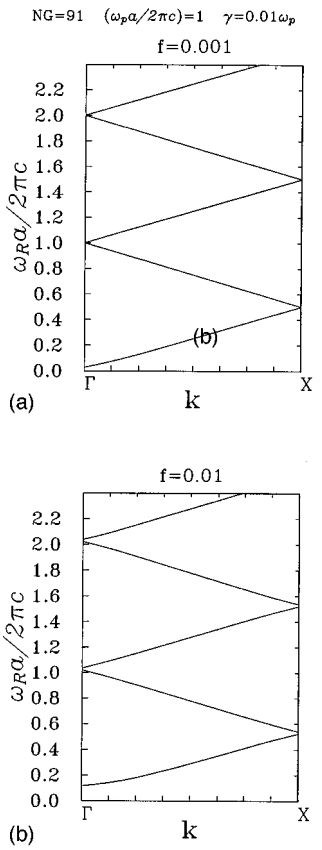

FIG. 5. The photonic band structure of a 1D lattice consisting of lossy metallic slabs in vacuum obtained by the perturbative plane-wave method. E polarization: (a) $f=0.001$ and (b) $f=0.01$. The number of plane waves used in these calculations is $NG=91$.

The imaginary part of the complex photonic band structures is represented by the lifetimes of the modes as determined from the imaginary parts of their frequencies ω_I, which correspond to the normalized complex frequency $\mu=\omega_R/c+i\omega_I/c$ according to the definition (2.11). In Figs. 6(a) and 6(b) we plot the lifetimes of the modes associated with the 12 lowest frequency bands on a logarithmic scale as a function of the wave number k for a 1D lattice formed by the metallic slabs in vacuum when the filling fraction $f=0.001$ and 0.01, respectively. The lifetime of the modes associated with the bands increases with increasing value of the wave number k, and displays a minimum at the Γ point $k=0$, where the strongest attenuation of the mode associated with the lowest band occurs. We display the lifetimes associated with the 12 lowest bands to demonstrate the fact that the lifetimes saturate to a finite value in the limit of large wave number k. The value of the lifetime at the Γ point is equal to the electron relaxation time τ_e given by the damping constant γ used in the dielectric function given by Eq. (1.1). The lifetimes associated with the modes at and above the plasma frequency are 10^2–10^3 times larger than the electron relaxation time, and are of the order of 10^{-11} and 10^{-10} s for the filling fractions $f=0.001$ and 0.01, respectively. A study of the dependence of the band structures on the damping constant γ indicates that the imaginary part is directly proportional to the value of the damping constant γ, unlike the real part, which does not vary significantly when the damp-

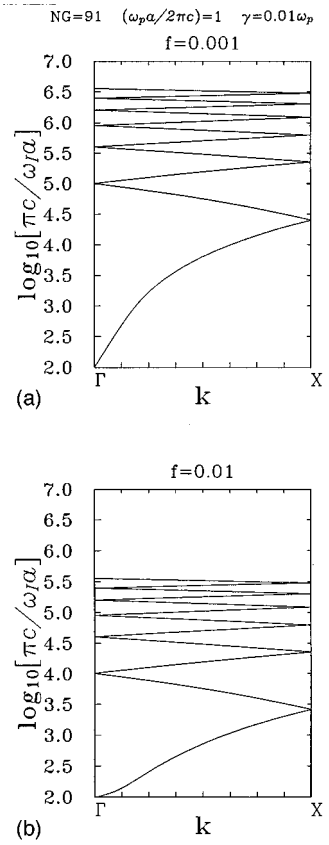

FIG. 6. The lifetime of the modes associated with the dispersion curves shown in Fig. 5. (a) $f=0.001$. (b) $f=0.01$.

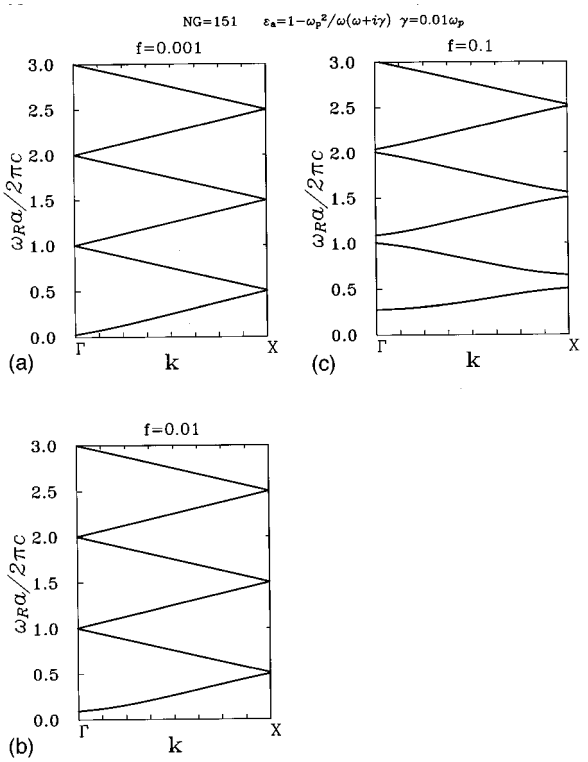

FIG. 7. The photonic band structure of a 1D lattice consisting of lossy metallic slabs in vacuum obtained by the linearization technique. *E* polarization: (a) $f=0.001$, (b) $f=0.01$, and (c) $f=0.1$. The number of plane waves used in these calculations is $NG=151$.

ing constant is changed. The convergence of the calculations of the band structure was monitored by increasing the number of the plane waves used in expansion (2.2). For small values of the filling fraction, $f\leqslant 1\%$, the use of a modest number of plane waves ~ 100 is sufficient to produce converged results.

Finally, we present the results obtained by the linearization scheme. In Figs. 7(a), 7(b), and 7(c), we plot the bands for the filling fractions $f=0.001$, 0.01, and 0.1, respectively. We monitored the convergence of these results by using up to 151 plane waves, which leads to the problem of diagonalizing a 453×453 complex matrix. The dispersion curves obtained clearly confirm the characteristic features of the photonic band structures of 1D metallic systems, such as the existence of the band gap below the lowest-frequency band and the structural band gaps for higher values of the filling fraction, and agree very well with the results calculated by using the transfer matrix method and the perturbative plane wave approach based on the reduction of the generalized eigenvalue problem to the problem of solving a set of coupled nonlinear equations. In contrast to the results obtained by the transfer matrix method, those displayed in Fig. 7 do not reveal the existence of the partial band below the lowest frequency band.

The diagonalization of the complex non-Hermitian matrix yields complex eigenvalues which correspond to the normalized complex frequency $\mu=\omega_R/c+i\omega_I/c$ defined by Eq. (2.9), and thus allow a direct comparison with those obtained by our perturbative plane wave approach. In Fig. 8 we plot the lifetimes of the modes in the extended-zone scheme on a logarithmic scale as functions of the wave number k. The lifetimes shown in Fig. 8 correspond to the frequency bands shown in Figs. 7(a)–7(c) for the filling fractions $f=0.001$, 0.01, and 0.1, respectively, and they exhibit identical behavior to that obtained by our perturbative plane wave approach, viz. they display a minimum at the Γ point which corresponds to the strongest attenuation for the lowest-frequency band. In addition, the lifetimes obtained by the linearization scheme also predict the existence of the asymmetrical behavior near the Brillouin-zone boundaries.

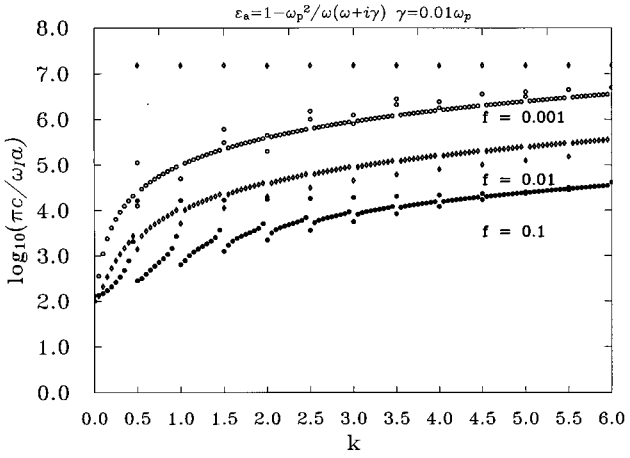

FIG. 8. The absorption coefficient of the modes associated with the photonic band structures displayed in Fig. 7, plotted in the extended zone scheme: $f=0.001$ (○○○○), $f=0.01$ (◇ ◇ ◇ ◇), and $f=0.1$(●●●●).

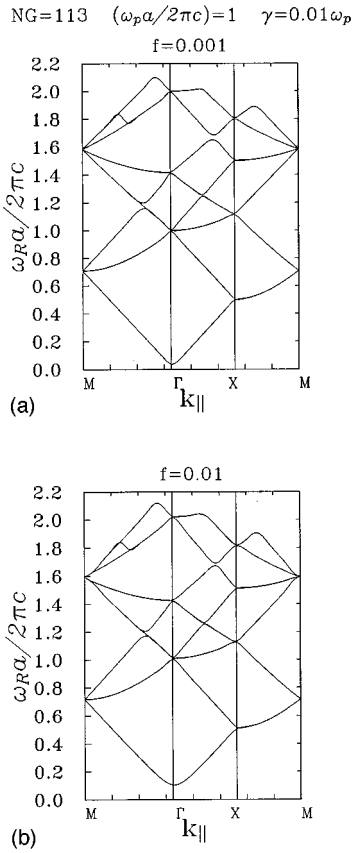

FIG. 9. The photonic band structure of a square lattice of lossy metal cylinders in vacuum obtained by the perturbative plane-wave method. E polarization: (a) $f=0.001$ and (b) $f=0.01$. The number of plane waves used in these calculations is $NG=113$.

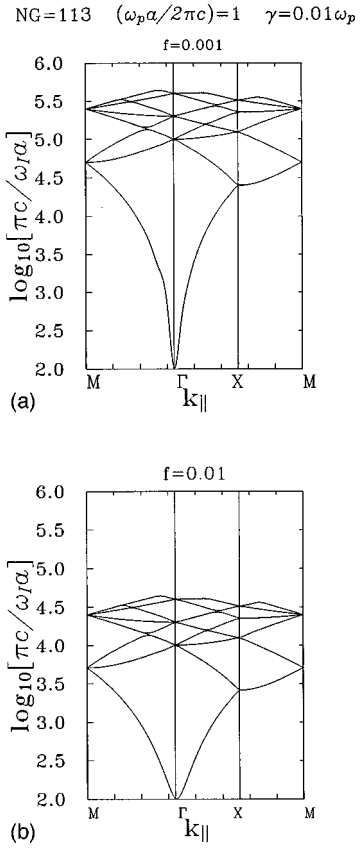

FIG. 10. The lifetime of the modes associated with the photonic band structures shown in Fig. 9. (a) $f=0.001$. (b) $f=0.01$.

In this case the asymmetry is represented by the increase of the lifetime of the mode with the frequency of the lower band edge at the Brillouin-zone boundary, and by the decrease of the lifetime of the mode with the frequency of the upper band edge at the Brillouin-zone boundary. The absorption coefficient and lifetime of a mode, as the complementary quantities characterizing the propagation of waves through 1D lossy metallic systems, provide consistent evidence of the anomalous behavior of the waves with frequencies in the neighborhood of the Brillouin-zone boundaries.

B. 2D systems

We first present the results obtained by using our perturbative plane-wave approach based on the reduction of the generalized eigenvalue problem to the problem of solving a set of coupled nonlinear equations. In Figs. 9(a) and 9(b), we plot the real part of the photonic band structures for E polarized electromagnetic waves propagating through a two-dimensional system consisting of lossy metallic rods arrayed in a simple square lattice of lattice constant a, when the filling fraction of the rods is $f=0.001$ and 0.01, respectively. We again assume $\omega_p a/2\pi c=1$. A total of 113 plane waves was used in obtaining these results. For both filling fractions considered, $f=0.001$ and 0.01, we obtained a band structure that is a slightly perturbed version of the dispersion relation for electromagnetic waves in vacuum, and which is in quantitative agreement with earlier results obtained by the present authors, where a simple free-electron dielectric function $\epsilon(\omega)$ without damping was used.[27] The calculated band structures also predict the existence of a band gap below the lowest-frequency band as a consequence of the metallic nature of the cylinders. The width of this gap is seen to increase with increasing filling fraction f. In Figs. 10(a) and 10(b), we plot the lifetimes of the modes on a logarithmic scale as functions of the wave vector $\mathbf{k}_\parallel$, for filling fractions $f=0.001$ and 0.01, respectively. As shown in these figures, the lifetimes of the modes as a function of the wave vector $\mathbf{k}_\parallel$ resemble the behavior of the associated real part of the photonic band structure, and display the strongest attenuation for the lowest band at the $\overline{\Gamma}$ point. The value of the lifetime at this point is equal to the electron relaxation time τ_e given by the damping constant γ used in the dielectric function $\epsilon(\omega)$. For frequencies $\omega>\omega_p$, the lifetimes are 10^3–10^2 times larger than the electron relaxation time, and are of the order of 10^{-10} and 10^{-11} s for the filling fractions $f=0.001$ and 0.01, respectively. The 2D photonic band structures display the same behavior as observed in the 1D case with respect to their dependence on the damping constant γ—the imaginary part is found to be directly proportional to the damping constant γ, unlike the real part, which does not vary significantly when the damping constant is changed. The convergence of the calculation of the band structures was monitored by increasing the number of the plane waves used in the expansions (3.7) and (3.12). For small values of the filling fraction, $f\leqslant 0.01$, the use of a modest number of plane waves, $NG\sim 100$, is sufficient to produce converged results.

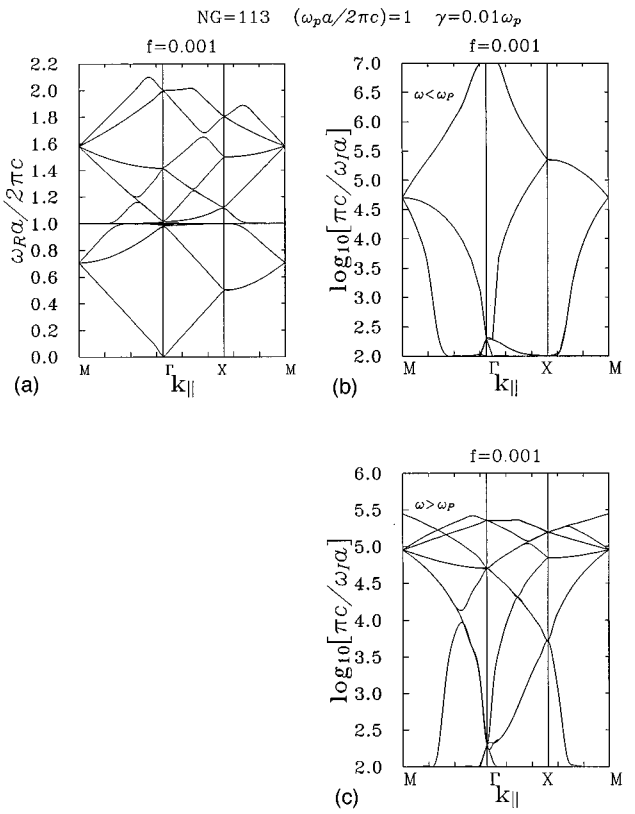

FIG. 11. (a) The photonic band structure of a square lattice of lossy metal cylinders in vacuum obtained by the perturbative plane wave approach. H polarization; $f=0.001$. (b) The lifetimes of the modes associated with this band structure whose frequencies are smaller than ω_p. (c) The lifetimes of the modes associated with this band structure whose frequencies are greater than ω_p. The number of plane waves used in these calculations is $NG=113$.

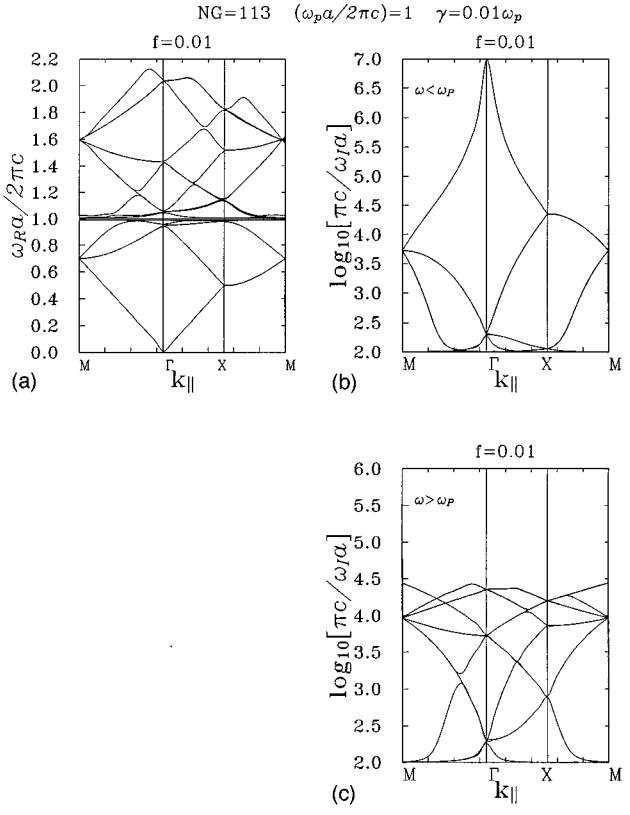

FIG. 12. The same as Fig. 11, except that $f=0.01$.

In Fig. 11(a) we present the real part of the photonic band structure for the case of H polarization for a square lattice, when the filling fraction of the rods is $f=0.001$. By solving the set of nonlinear equations (3.21a) and (3.21b), we have found two independent solutions for each band for a given wave vector $\mathbf{k}_\parallel$. The solutions represent two qualitatively different parts of the photonic band structure, namely, a nearly dispersionless one, which is consistent with the existence of the flatbands in the region $0<\omega<\omega_p$ reported recently,[27] and a dispersive part of the photonic band structure which resembles the dispersion relation for electromagnetic waves in vacuum. The convergence of the calculation of the band structure was monitored by increasing the number of plane waves used in expansion (3.18). Since the convergence of these calculations for small values of the filling fraction, $f\leqslant 0.01$, is rapid, relatively small matrices $NG\sim 100$ were required for an accurate determination of the dispersive part of the photonic band structure. In fact, a total of 113 plane waves was used in obtaining these results. As is known from our earlier calculations,[24,27] the convergence of the flatbands is significantly slower than the convergence of the dispersive part of the photonic band structure, and the use of a large number of plane waves together with an extrapolation procedure is required to obtain accurate results. Taking into account that the eigenvalues converge asymptotically with increasing number of plane waves, and the inherent inaccuracy associated with the perturbative approach used, the calculated flatbands should be regarded only as indicative of the true flat band structure that exists in the frequency range $0<\omega<\omega_p$.

In Figs. 11(b) and 11(c), we plot the lifetimes of these modes on a logarithmic scale as functions of the wave vector $\mathbf{k}_\parallel$. The lifetimes of the modes with frequencies greater than ω_p are essentially proportional to the wave vector $\mathbf{k}_\parallel$, while the lifetimes of the modes with frequencies below ω_p are essentially inversely proportional to the wave vector $\mathbf{k}_\parallel$. Hence the lifetimes of the modes from both the frequency regions below and above ω_p are larger than those associated with the flatbands, which yield a global minimum of the lifetime of the complete photonic band structure.

In Fig. 12(a) we present the real part of the photonic band structure for the case of H polarization for a square lattice, when the filling fraction of the rods is $f=0.01$, obtained by solving the set of nonlinear equations. In Figs. 12(b) and 12(c) we plot the lifetimes of these modes on a logarithmic scale as functions of the wave vector $\mathbf{k}_\parallel$ for modes with frequencies smaller and greater than ω_p, respectively. The calculations whose results are presented in these figures were carried out exactly in the same way as were the calculations whose results are presented in Fig. 11, and the results are qualitatively very similar to those for a lower filling fraction. Quantitatively, the lifetimes of the modes corresponding to the filling fraction $f=0.01$ are smaller than the lifetimes of the modes calculated for $f=0.001$, which is consistent with the expected fact that the modes become more attenuated as the filling fraction of the rods increases.

We now turn to the results for both polarizations obtained by the linearization technique described in Sec. III A 2 and

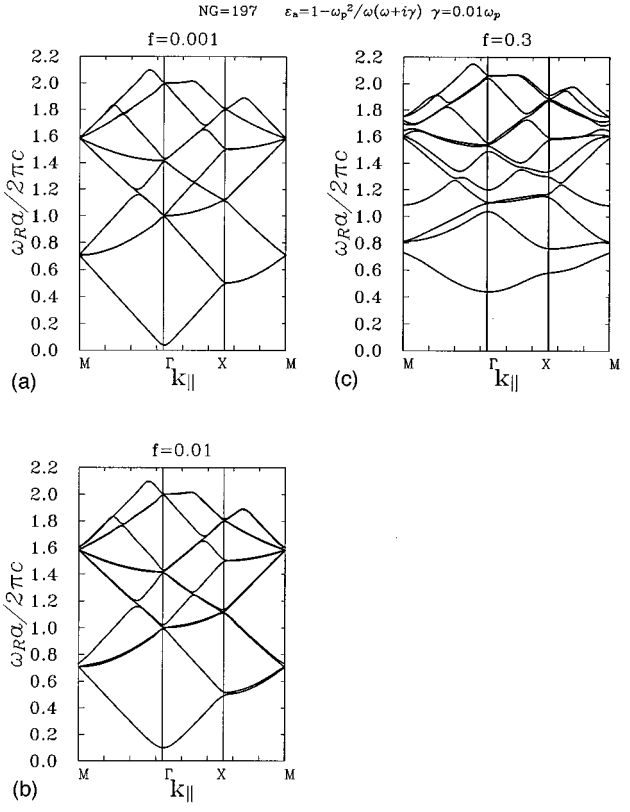

FIG. 13. The photonic band structure of a square lattice of lossy metal cylinders in vacuum obtained by the linearization technique. E polarization: (a) $f=0.001$, (b) $f=0.01$, and (c) $f=0.3$. The number of plane waves used in these calculations is $NG=197$.

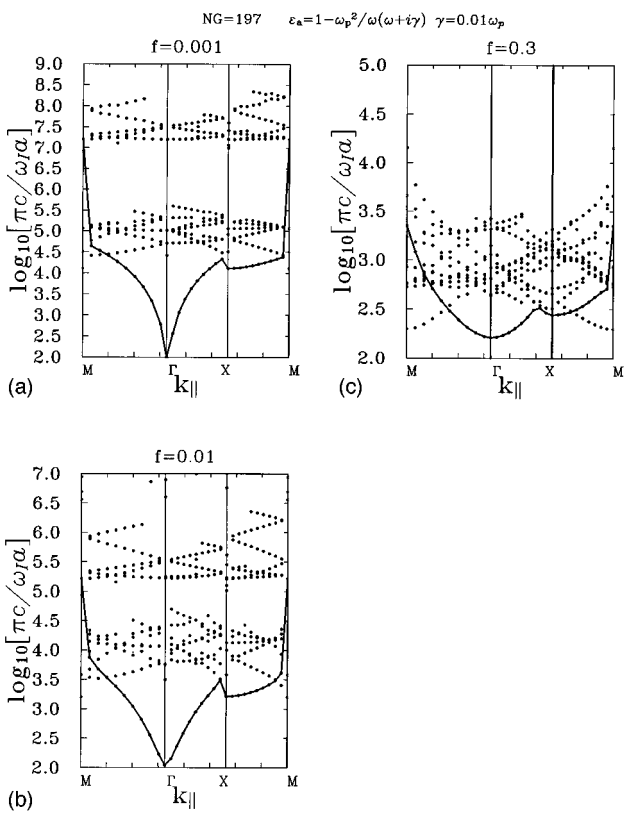

FIG. 14. The lifetime of the modes associated with the photonic band structures shown in Fig. 13. (a) $f=0.001$. (b) $f=0.01$. (c) $f=0.3$.

III B 2. In Figs. 13(a) and 13(b), we plot the frequency bands for E-polarized electromagnetic waves propagating through the system of lossy metallic rods arrayed in a simple square lattice with the filling fractions $f=0.001$ and 0.01, respectively. The dispersion curves obtained are identical with those calculated by using our perturbative plane-wave approach based on solving a set of coupled nonlinear equations. In addition, the linearization technique allows calculating the photonic band structures of systems with higher filling fractions of the rods, as is shown in Fig. 13(c), where the real part of the photonic band structure for E-polarized electromagnetic waves for the filling fraction $f=0.3$ is depicted. This photonic band structure displays a typical behavior of the dispersion curves for systems containing metallic elements which, for higher values of the filling fraction, predict, besides the gap below the lowest-frequency band, a structural one between the first and the second bands. We note that the presence of damping does not affect the dispersion relation for electromagnetic waves propagating through 2D metallic systems in comparison with that determined for the identical systems characterized by a lossless free electron dielectric function.[27] We used 197 plane waves in obtaining these results. The convergence of the results for higher values of the filling fraction was monitored by using up to 529 plane waves.

The lifetimes of the E-polarized modes are determined from the imaginary part of the complex eigenvalues obtained by diagonalizing the non-Hermitian matrix given by Eq. (3.17). In Figs. 14(a)–14(c), we present the lifetimes associated with the 12 lowest bands plotted in Figs. 13(a)–13(c), which correspond to the filling fractions $f=0.001$, 0.01, and 0.3, respectively. The results shown in these figures agree qualitatively with those obtained by our perturbative plane-wave method. However, they reveal additional features such as the asymmetric behavior near the Brillouin-zone boundaries—indicated in Figs. 14(a)–14(c) by a full line—for the lowest-frequency mode, and an anomalous behavior of the lifetimes associated with the frequency bands which are degenerate along the high-symmetry directions in the Brillouin zone. For the sake of clarity of the figures in which the lifetimes in the presence of singular behavior near the Brillouin zone boundaries are shown, we use dotted lines to plot them. In fact, the lifetimes associated with the twofold-degenerate bands are split into two different branches, which correspond to symmetric and asymmetric modes, respectively. The splitting of these modes is demonstrated in Figs. 14(a) and 14(b), in which both types of modes associated with the 12 lowest bands form two different regions of the lifetimes. The results shown in Figs. 14(a)–14(c) also indicate that the values of the lifetimes decrease as the filling fraction is increased. We observed that for higher values of the filling fraction—see Fig. 14(c)—the lifetimes of the degenerate modes display different behavior which, however, does not result in the existence of separated branches of the lifetimes, as is observed for lower values of the filling fraction. We again suggest that the origin of the anomalous behavior of the lifetime near the Brillouin-zone boundaries is the redistribution of the electromagnetic field for modes at the top and the bottom of a gap as we proposed in the context

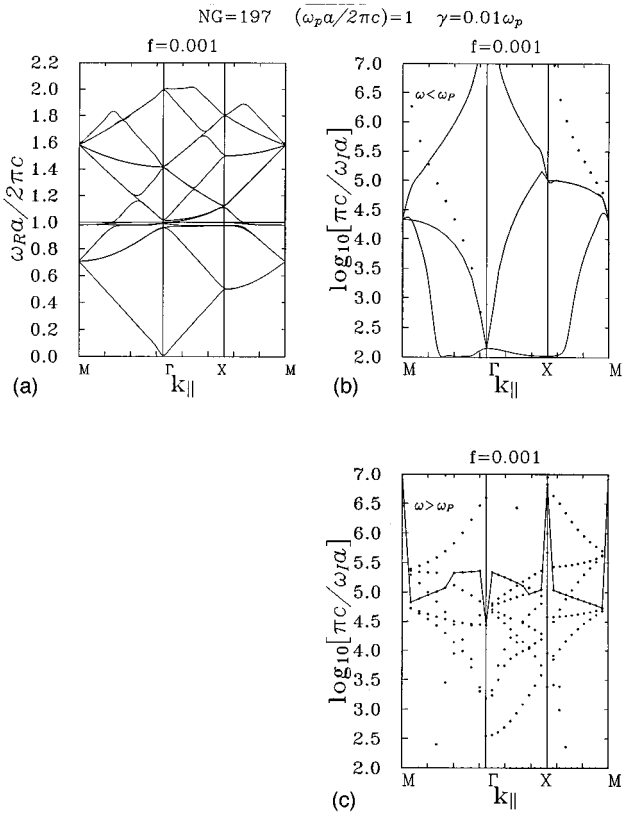

FIG. 15. (a) The photonic band structure of a square lattice of lossy metal cylinders in vacuum obtained by the linearization technique. H polarization, $f=0.001$. (b) The lifetimes of the modes associated with this band structure whose frequencies are smaller than ω_p. (c) The lifetimes of the modes associated with this band structure whose frequencies are greater than ω_p. The number of plane waves used in these calculations is $NG=197$.

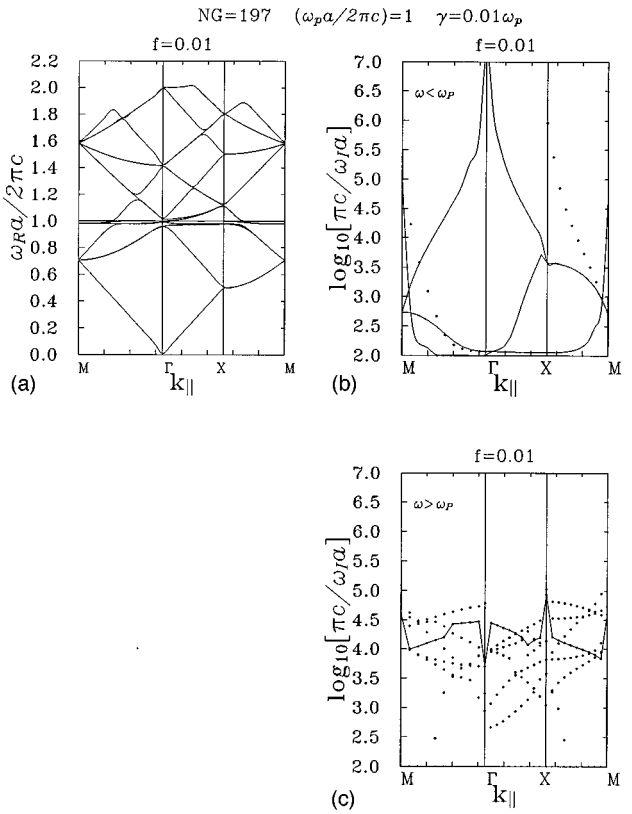

FIG. 16. The same as Fig. 15, except that $f=0.01$.

of the one-dimensional system in Sec. IV A. The existence of the different lifetimes associated with the degenerate modes can possibly be related to the interaction between the modes which removes the degeneracy in the imaginary part of the complex frequency. However, further theoretical analysis is needed to provide the full physical explanation of this effect.

In Figs. 15(a), 16(a), and 17(a), we demonstrate the profoundly different behavior of the dispersion curves for H-polarized electromagnetic waves propagating through the same two-dimensional system for the filling fractions $f=0.001$, 0.01, and 0.1, respectively. They confirm the existence of the flatbands below the plasma frequency ω_p which have been identified as due to the overlap of H-polarized excitations associated with an isolated metallic cylinder.[27] It is interesting to note that the dispersion curves obtained by the linearization scheme exhibit a wider range of the frequencies in which the flatbands occur in comparison with those obtained by using our perturbative plan-wave approach described in Sec. III B 1, and they provide clear evidence of the strong interaction of the free-space dispersion relation with the flat modes. The lifetimes of the H-polarized modes propagating through the two-dimensional system with the filling fractions $f=0.001$, 0.01, and 0.1 are shown in Figs. 15(b) and 15(c), 16(b) and 16(c), and 17(b) and 17(c). In agreement with the lifetimes obtained by our

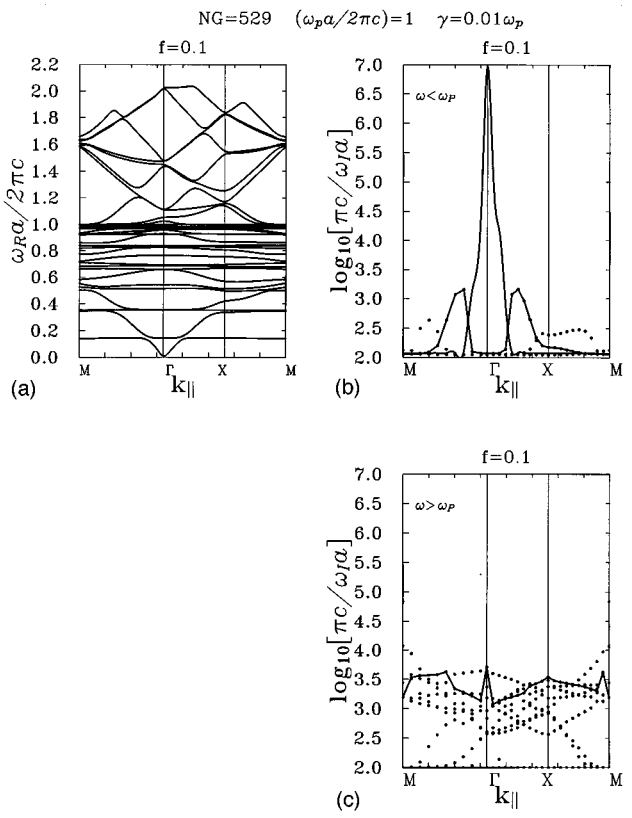

FIG. 17. The same as Fig. 11, except that $f=0.1$. The number of plane waves used in these calculations is $NG=529$.

perturbative plane-wave approach, they also reveal direct (inverse) proportionality to the wave vector $\mathbf{k}_\parallel$ of the lifetime associated with the modes with frequencies above (below) the plasma frequency ω_p, while the minimum of the lifetime given by the damping constant γ is associated with the flatbands. As the most striking feature of these results, the lifetimes obtained by the linearization scheme in contrast to those obtained by our perturbative plane-wave method display substantially different dependences on the wave vector $\mathbf{k}_\parallel$ in the frequency ranges along the high-symmetry directions in which the associated modes are degenerate, and in their singular behavior near the Brillouin-zone boundaries. The latter effect is indicated in Figs. 15(c), 16(c) and 17(c) by the full line for the highest-frequency mode, while the splitting of the lifetimes associated with the degenerate modes along the $M-\Gamma$ and $X-M$ directions is indicated by the dotted lines in Figs. 15(b) and 16(b). The existence of the different lifetimes associated with the degenerate frequency modes was not observed for higher values of the filling fraction for frequencies below ω_p—see Fig. 17(b)—because the photonic band structure in this frequency range is dominated by the presence of the flatbands.

V. DISCUSSION AND CONCLUSIONS

In this paper we calculated the photonic band structures of electromagnetic waves propagating through periodic one- and two-dimensional systems containing components characterized by the complex, frequency-dependent, dielectric function given by Eq. (1.1), which accounts for the dissipative behavior of real lossy metallic materials. We developed an interesting approach within the framework of the plane-wave approximation, based on the reduction of a generalized eigenvalue problem to the problem of solving sets of coupled nonlinear equations. We demonstrated that for low filling fractions this perturbative plane-wave method provides a computationally viable alternative to the computer-intensive linearization method for calculating the photonic band structures of both one- and two-dimensional periodic systems containing lossy metallic components. The calculated complex photonic band structures yield both the dispersion curves and the lifetimes of the modes associated with the bands. Besides the perturbative plane wave technique, for the 1D system we also used the transfer-matrix method, which yields an explicit, analytic, dispersion relation that can be used to assess the accuracy and the reliability of the variants of the plane-wave method. The results obtained by the transfer-matrix method, except for the existence of an additional band below the lowest-frequency band, agree very well for the most part with those obtained by both our approach and the linearization scheme. This discrepancy indicates, that the singular behavior of the dielectric function for a metal given by Eq. (1.1) at the pole $\omega=0$ and, consequently, the mutual interaction of both the real and imaginary parts of the dispersion relation at this point is not sufficiently accurately described within the plane-wave approximation used in both methods, and thus does not account for the additional modes below the lowest frequency band.

The dispersion curves obtained by our perturbative plane-wave approach and the linearization technique for the photonic band structures of periodic arrays of lossy metallic slabs (rods) embedded in vacuum are not significantly different from the dispersion curves for electromagnetic waves in vacuum, and agree qualitatively with the results obtained by using a simple free-electron model dielectric function in the absence of damping.[27] The photonic band structures of EM waves of E polarization, in addition to possessing a structural gap between the higher-frequency bands, which appears for the values of the filling fraction $f \gtrsim 0.25$, possess an absolute band gap below the lowest-frequency band, whose dispersion curve does not tend to zero frequency at the Γ ($\bar{\Gamma}$) point. The width of this gap increases with increasing filling fraction. Such a gap is not observed in the 1D structures consisting of dielectric slabs, and in 2D systems when the metal cylinders are replaced by dielectric cylinders, and is a consequence of the metallic nature of the components. Both our perturbative plane-wave approach and the linearization method employed for the calculation of the photonic band structures of EM waves of H polarization propagating in a system of metallic rods in the presence of dissipation produce results that are nearly identical to those found in the absence of damping. The dispersion curves do not possess a band gap below the lowest-frequency band, and confirm the existence of additional, nearly dispersionless, bands in the frequency range $\omega<\omega_p$, effectively superimposed on the dispersive part of the band structures. We have found that the flatbands strongly interact with the free-space dispersion curves, and act as traps for energy entering the system through the free-space wave. These features clearly demonstrate the differences between the band structures for different polarizations of the waves, and provide an explanation for the well-known fact that a conducting wire system can act as a polarizer which transmits EM waves of H polarization at low frequencies, but not waves of E polarization.

By using the transfer-matrix method and both plane-wave techniques, we determined from the imaginary part of the resulting photonic band structures the absorption coefficient and the lifetime of the modes as complementary quantities which characterize the modes as they propagate through the system. Except in the frequency regions near the Brillouin-zone boundaries, both the absorption coefficient and the lifetime exhibit a monotonic behavior, displaying a global extremum at the Γ point, yielding the smallest lifetime and the largest absorption coefficient for the lowest-frequency band. Both the absorption coefficient and the lifetime of the modes display an asymmetric behavior in the neighborhood of the band edges. We note that although the asymmetry of the lifetime, which is consistent with that of the absorption coefficient, is predicted by the linearization scheme, it is, however, not found in the results of our perturbative plane-wave method. Even if we take into account that the asymmetric behavior is negligible for small filling fractions, the absence of such features for the lifetime of the modes suggests that our approximation does not give the correct picture due to the (near) degeneracy of the bands in the neighborhood of the gaps. We have proposed an explanation of this effect as caused by the redistribution of the electromagnetic field in the modes at the top and bottom of a gap. Considering that a metal acts as a reflecting potential, the smaller absorption and longer lifetime of modes at the bottom of the gap is due to the minimized overlap of the associated photon wave

function with the metal. The reverse is true for modes at the top of the band, where the overlap between the field and the metal is maximized and, therefore, the absorption is larger and the lifetime is shorter.

The asymmetric behavior observed for both the absorption coefficient and the lifetime of the modes provides an interesting example of a more general phenomenon associated with the properties of the electromagnetic wave propagation near the Brillouin-zone edges, and it is therefore of interest to study this effect further in the context of the anomalous behavior of the absorption coefficient which occurs due to the fundamental change in the nature of transport through a disordered medium, and which was suggested as a probe for the existence of a photon mobility edge.[40,41]

The results for E-polarized EM waves obtained by our perturbative plane-wave approach in both 1D and 2D periodic systems indicate that the modes associated with the lowest-frequency band are the most strongly attenuated, and that their lifetime tends to the value of the conduction electron relaxation time τ_e at the Γ ($\bar{\Gamma}$) point. The lifetimes of the modes as functions of the wave vector k ($\mathbf{k}_\parallel$) resemble the behavior of the associated real part of the photonic band structures, and display the strongest attenuation for the lowest frequency band at the Γ ($\bar{\Gamma}$) point. The difference between the lifetimes of the modes of the lowest frequency band and the lifetimes of the modes with frequencies ω above ω_p decreases as the filling fraction of the slabs (cylinders) increases. A quite different dependence is observed for the attenuation of the modes as a function of the wave vector $\mathbf{k}_\parallel$ for H-polarized EM waves propagating through a 2D array of lossy metal rods. The attenuation of the flatbands also exhibits nearly dispersionless behavior, and the corresponding lifetimes of these modes are found to be close to the electron relaxation time τ_e, which corresponds to the bands at the plasma frequency ω_p. The lifetimes of the modes in the dispersive part of the photonic band structure with frequencies above ω_p are proportional to the wave vector $\mathbf{k}_\parallel$, while the lifetimes associated with the modes with frequencies below ω_p are inversely proportional to the wave vector $\mathbf{k}_\parallel$. Thus the lifetimes of the modes with frequencies from both regions are larger than those associated with the flatbands.

Rather more striking behavior is revealed by the results for the lifetimes of both the E- and H-polarized modes in 2D systems obtained by using the linearization technique. They agree qualitatively with those obtained by using our perturbative plane-wave approach. However, they display additional features such as an asymmetric behavior near the Brillouin-zone boundaries and the splitting of the lifetimes associated with the twofold-degenerate modes along high-symmetry directions in the Brillouin zone. The origin of the former effect was identified as the redistribution of the electromagnetic field in the modes at the bottom and top of a gap. The existence of the different lifetimes associated with degenerate modes can be understood in terms of the interaction of the modes, which removes the degeneracy in the imaginary part of the complex frequency. A detailed explanation of this effect, however, requires further theoretical investigation.

Studies in progress focus on the photonic band structures of a periodic array of slabs (rods) fabricated from a lossy polar semiconductor whose dielectric function has the form

$$\epsilon(\omega)=\epsilon_i+(\epsilon_0-\epsilon_i)\frac{\omega_T^2}{\omega_T^2-\omega^2-i\Gamma\omega}, \tag{5.1}$$

where ϵ_0 is the static dielectric constant, ϵ_i is the optical frequency dielectric constant, ω_T is the frequency of the transverse optical mode of infinite wavelength, and Γ is a damping constant. In this case the Maxwell equations can be transformed into a generalized eigenvalue problem. This problem can be solved by using the linearization scheme, based on the construction of an equivalent enlarged matrix and, for structures with small filling fractions, the approach requiring the solution of sets of nonlinear equations developed in this paper can also be used.

We also plan to study the distribution of the electromagnetic field in terms of the eigenmodes which correspond to the individual frequency bands. By evaluating the group velocity of each eigenmode, the flow of energy will be examined. Then we intend to study the symmetry of the modes found by diagonalizing a complex, non-Hermitian matrix. In particular, the symmetry of the photon waves which correspond to the lower and upper edges of the band gaps and those associated with the degenerate bands in two-dimensional photonic band structures will be studied to acquire deeper physical insight into the nature of the phenomena associated with the imaginary component of the complex photonic band structures.

ACKNOWLEDGMENTS

The work of V.K. was supported in part by the Grant of the Czech Academy of Sciences No. 202/96/1239. The work of A.A.M. was supported in part by NSF Grant No. DMR93-19404. This research was also supported by the University of California, Irvine, through an allocation of computer time.

*Permanent Address: Institute of Radio Engineering and Electronics, Czech Academy of Sciences, Chaberska 57, 182 51 Prague 8, Czech Republic.

[1] See the papers in the special issue of J. Opt. Soc. Am. B **10**(2) on Development and Applications of Materials Exhibiting Photonic Band Gaps, edited by C. M. Bowden, J. P. Dowling, and H. O. Everitt, pp. 279–413 (1993).

[2] E. Yablonovitch, Phys. Rev. Lett. **58**, 2059 (1987).

[3] M. Plihal, A. Shambrook, A. A. Maradudin, and P. Sheng, Opt. Commun. **50**, 199 (1991).

[4] M. Plihal and A. A. Maradudin, Phys. Rev. B **44**, 8565 (1991).

[5] P. R. Villneuve and M. Piché, J. Opt. Soc. Am. A **8**, 1296 (1991).

[6] S. L. McCall, P. M. Platzman, R. Dalichaouch, D. R. Smith, and S. Schultz, Phys. Rev. Lett. **67**, 2017 (1991).

[7] R. D. Meade, K. D. Brommer, A. M. Rappe, and J. D. Joannopoulos, Appl. Phys. Lett. **61**, 495 (1992).

[8] P. R. Villneuve and M. Piché, Phys. Rev. B **46**, 4969 (1992).

[9] P. R. Villneuve and M. Piché, Phys. Rev. B **46**, 4973 (1992).

[10] J. B. Pendry and A. MacKinnon, Phys. Rev. Lett. **69**, 2772 (1992).

[11] A. A. Maradudin and A. R. McGurn, J. Opt. Soc. Am. B **10**, 307 (1993).

[12] D. R. Smith, R. Dalichaouch, N. Kroll, S. Schultz, S. L. McCall, and P. M. Platzman, J. Opt. Soc. Am. B **10**, 314 (1993).
[13] R. D. Meade, A. M. Rappe, K. D. Brommer, and J. D. Joannopoulos, J. Opt. Soc. Am. B **10**, 328 (1993).
[14] D. L. Bullock, C.-C. Shih, and R. S. Margulies, J. Opt. Soc. Am. B **10**, 399 (1993).
[15] K. M. Leung and Y. Qiu, Phys. Rev. B **48**, 7767 (1993).
[16] R. D. Meade, A. M. Rappe, K. D. Brommer, J. D. Joannopoulos, and O. L. Alerhand, Phys. Rev. B **48**, 8434 (1993).
[17] A. A. Maradudin and A. R. McGurn, in *Photonic Band Gaps and Localization*, edited by C. M. Soukoulis (Plenum, New York, 1993), p. 247.
[18] J. N. Winn, R. D. Meade, and J. D. Joannopoulos, J. Mod. Opt. **41**, 257 (1994).
[19] A. A. Maradudin and A. R. McGurn, J. Mod. Opt. **41**, 275 (1994).
[20] R. D. Meade, A. Devenyi, J. D. Joannopoulos, O. L. Alerhand, D. A. Smith, and K. Kash, J. Appl. Phys. **75**, 4753 (1994).
[21] W. Robertson, G. Arjavalingam, R. D. Meade, K. D. Brommer, A. M. Rappe, and J. D. Joannopoulos, Phys. Rev. Lett. **68**, 2033 (1992).
[22] W. Robertson, G. Arjavalingam, R. D. Meade, K. D. Brommer, A. M. Rappe, and J. D. Joannopoulos, J. Opt. Soc. Am. B **10**, 333 (1993).
[23] S. Schultz and D. R. Smith, in *Photonic Band Gaps and Localization* (Ref. 17), p. 305.
[24] A. R. McGurn and A. A. Maradudin, Phys. Rev. B **48**, 17 576 (1993).
[25] M. M. Sigalas, C. M. Soukoulis, E. N. Economou, C. T. Chan, and K. M. Ho, Phys. Rev. B **48**, 14 121 (1993).
[26] M. M. Sigalas, C. M. Soukoulis, C. T. Chan, and K. M. Ho, Phys. Rev. B **49**, 11 080 (1994).
[27] V. Kuzmiak, A. A. Maradudin, and F. Pincemin, Phys. Rev. B **50**, 16 835 (1994).
[28] A. A. Maradudin, V. Kuzmiak, and A. R. McGurn, in *Photonic Band Gap Materials*, edited by C. M. Soukoulis (Kluwer, Dordrecht, 1996), p. 271.
[29] V. Kuzmiak and A. A. Maradudin, in *Photonic Band Gap Materials* (Ref. 28), p. 319.
[30] J. B. Pendry, J. Mod. Opt. **41**, 209 (1994).
[31] T. Suzuki and P. K. L. Yu, J. Opt. Soc. Am. B **12**, 583 (1994).
[32] A. J. Ward, J. B. Pendry, and W. J. Stewart, J. Phys. C **7**, 2217 (1995).
[33] M. M. Sigalas, C. T. Chan, K. M. Ho, and C. M. Soukoulis, Phys. Rev. B **52**, 11 744 (1995).
[34] K. Inoue, M. Wada, K. Sakoda, A. Yamanaka, M. Hayashi, and J. W. Haus, Jpn. J. Appl. Phys. **33**, L1436 (1994).
[35] K. Inoue, M. Wada, K. Sakoda, M. Hayashi, T. Fukushima, and A. Yamanaka, Phys. Rev. B **53**, 1010 (1996).
[36] P. Lancaster, *Lambda-Matrices and Vibrating Systems* (Pergamon, London, 1996), Chap. 4.
[37] G. Peters and J. H. Wilkinson, SIAM J. Appl. Math. **7**, 479 (1970).
[38] Pochi Yeh, *Optical Waves in Layered Media* (Wiley, New York, 1988), p. 125.
[39] S. Wolfram, MATHEMATICA (Addison-Wesley, Reading, MA, 1988).
[40] S. John, Phys. Rev. Lett. **58**, 2486 (1987).
[41] S. John, Phys. Today **44**(5), 32 (1991).